

Dosimetric impact of interplay effects in  
Stereotactic Body Radiation Therapy (SBRT) lung cancer



A Dissertation Submitted in Partial Fulfillment of the Requirements  
for the Degree of Doctor of Philosophy in Medical Physics

Department of Radiology

FACULTY OF MEDICINE

Chulalongkorn University

Academic Year 2021

Copyright of Chulalongkorn University

ผลทางรังสีต่อสภาวะอินเทอร์เน็ตเพลย์สำหรับผู้ป่วยมะเร็งปอด  
ที่ได้รับการรักษาด้วยเทคนิครังสีร่วมฟกัคบริเวณลำตัว



วิทยานิพนธ์นี้เป็นส่วนหนึ่งของการศึกษาตามหลักสูตรปริญญาวิทยาศาสตรดุษฎีบัณฑิต  
สาขาวิชาฟิสิกส์การแพทย์ ภาควิชารังสีวิทยา  
คณะแพทยศาสตร์ จุฬาลงกรณ์มหาวิทยาลัย  
ปีการศึกษา 2564  
ลิขสิทธิ์ของจุฬาลงกรณ์มหาวิทยาลัย

Thesis Title	Dosimetric impact of interplay effects in Stereotactic Body Radiation Therapy (SBRT) lung cancer
By	Miss Vanida Poolnapol
Field of Study	Medical Physics
Thesis Advisor	Assistant Professor Taweap Sanghangthum, Ph.D.

---

Accepted by the FACULTY OF MEDICINE, Chulalongkorn University in Partial Fulfillment of the Requirement for the Doctor of Philosophy

..... Dean of the FACULTY OF MEDICINE  
(Associate Professor Chanchai Sittipunt, M.D.)

DISSERTATION COMMITTEE

..... Chairman  
(Associate Professor Anchali Krisanachinda, Ph.D.)

..... Thesis Advisor  
(Assistant Professor Taweap Sanghangthum, Ph.D.)

..... Examiner  
(Mintra Keawsamur, Ph.D.)

..... Examiner  
(Sornjarod Oonsiri, Ph.D.)

..... Examiner  
(Anussara Prayongrat, M.D., Ph.D.)

..... External Examiner  
(Professor Franco Milano, Ph.D.)

วรรณิศา พูลนาผล : ผลทางรังสีต่อสภาวะอินเตอร์เพลย์สำหรับผู้ป่วยมะเร็งปอดที่ได้รับการรักษาด้วยเทคนิครังสีร่วมพิกัดบริเวณลำตัว. ( Dosimetric impact of interplay effects in Stereotactic Body Radiation Therapy (SBRT) lung cancer) อ.ที่ปรึกษาหลัก : อ. ดร.ทวีป แสงแห่งธรรม

การหายใจของผู้ป่วยมะเร็งปอดส่งผลทำให้เกิดผลทางรังสีต่อสภาวะอินเตอร์เพลย์ในขณะที่ได้รับการฉายรังสีแบบปรับความเข้มแบบหมุนรอบตัวร่วมด้วยเทคนิครังสีร่วมพิกัดบริเวณลำตัว ซึ่งสามารถนำไปสู่การเกิดปริมาณรังสีที่ไม่สม่ำเสมอภายในก้อนมะเร็งและเนื้อเยื่อรอบข้างได้ ดังนั้นวัตถุประสงค์ของงานวิจัยนี้จัดทำขึ้นเพื่อศึกษาผลทางรังสีต่อสภาวะอินเตอร์เพลย์สำหรับผู้ป่วยมะเร็งปอดที่ได้รับการรักษาด้วยแผนการรักษาแบบสามมิติที่ใช้รังสีโฟตอนพลังงาน 6 เมกะโวลต์ ร่วมกับเทคนิคการฉายรังสีแบบไม่ใช้แผ่นกรองลำรังสี และเพื่อหาปัจจัยใหม่ที่สามารถคำนวณผลทางรังสีต่อสภาวะอินเตอร์เพลย์สำหรับผู้ป่วยมะเร็งปอดที่ได้รับการรักษาด้วยเทคนิคการฉายรังสีแบบปรับความเข้มแบบหมุนรอบตัวร่วมด้วยเทคนิครังสีร่วมพิกัดบริเวณลำตัวได้โดยตรง ในงานวิจัยนี้จะเปรียบเทียบปริมาณรังสีในสภาวะหยุดนิ่งและสภาวะเคลื่อนไหวของหุ่นจำลอง โดยใช้หุ่นจำลองที่สามารถเคลื่อนที่ได้สองทิศทางร่วมกับอาร์เรย์ไดโอดในแผนการรักษาแบบสามมิติ และใช้หุ่นจำลองที่สามารถเคลื่อนที่ได้สามทิศทางร่วมกับฟิล์มและหัวเครื่องซินติไลออนในเซชันในแผนการรักษาด้วยเทคนิคการฉายรังสีแบบปรับความเข้มแบบหมุนรอบตัวร่วมด้วยเทคนิครังสีร่วมพิกัดบริเวณลำตัว สำหรับผลการทดลองในแผนการรักษาแบบสามมิติ พบว่าเปอร์เซ็นต์แกมมา 1 เปอร์เซ็นต์ 1 มิลลิเมตรจะลดลงเมื่อแอมพลิจูดของการหายใจเพิ่มขึ้น อย่างไรก็ตามเปอร์เซ็นต์แกมมากลับเพิ่มขึ้นสำหรับขนาดลำรังสีที่เพิ่มขึ้น ส่วนปัจจัยอื่น ๆ ไม่พบความเปลี่ยนแปลง ส่วนผลการทดลองในแผนการด้วยเทคนิคการฉายรังสีแบบปรับความเข้มแบบหมุนรอบตัวร่วมด้วยเทคนิครังสีร่วมพิกัดบริเวณลำตัว พบว่าแอมพลิจูดของการหายใจที่เพิ่มขึ้น ทิศทางการเคลื่อนที่ของก้อนมะเร็งที่เพิ่มมากขึ้นและปริมาณรังสีที่ลดลงจะส่งผลกระทบต่อสภาวะอินเตอร์เพลย์ ดังนั้นสามปัจจัยนี้จึงเป็นปัจจัยในการคำนวณค่า interplay effects factor (IEF) และจากการคำนวณพบว่า 10.13 เป็นตัวเลขที่เหมาะสมที่จะใช้เป็นจุดตัดในการพิจารณาใช้การจัดการเรื่องการหายใจรูปแบบใดรูปแบบหนึ่งของผู้ป่วยมะเร็งปอดที่ได้รับการรักษาด้วยเทคนิคการฉายรังสีแบบปรับความเข้มแบบหมุนรอบตัวร่วมด้วยเทคนิครังสีร่วมพิกัดบริเวณลำตัว โดยสรุปผลทางรังสีจากสภาวะอินเตอร์เพลย์ในแผนการรักษาด้วยรังสีโฟตอนพลังงาน 6 เมกะโวลต์ ร่วมกับเทคนิคการฉายแบบไม่ใช้แผ่นกรองลำรังสีในผู้ป่วยมะเร็งปอดที่ได้รับการรักษาด้วยเทคนิคการฉายรังสีแบบปรับความเข้มแบบหมุนรอบตัวร่วมด้วยเทคนิครังสีร่วมพิกัดบริเวณลำตัวจะมีผลกระทบเพิ่มขึ้นเมื่อแอมพลิจูดของการหายใจและทิศทางของก้อนมะเร็งปอดเพิ่มขึ้นและปริมาณรังสีลดลง โดยแอมพลิจูดของการหายใจที่สูงกว่า 5 มิลลิเมตร สามารถนำไปสู่การเปลี่ยนแปลงรูปร่างของการกระจายตัวของปริมาณรังสีอย่างมีนัยสำคัญเนื่องจากสภาวะอินเตอร์เพลย์ที่เกิดขึ้น โดยเฉพาะอย่างยิ่งสำหรับการเคลื่อนที่สามทิศทางของก้อนมะเร็ง และในงานวิจัยนี้ได้ค้นพบค่า IEF ซึ่งเป็นปัจจัยใหม่ที่สามารถบ่งชี้ถึงผลทางรังสีต่อสภาวะอินเตอร์เพลย์ได้โดยตรงสำหรับผู้ป่วยมะเร็งปอดที่ได้รับการรักษาด้วยเทคนิคการฉายรังสีแบบปรับความเข้มแบบหมุนรอบตัวร่วมด้วยเทคนิครังสีร่วมพิกัดบริเวณลำตัว โดยค่า IEF เท่ากับ 1 คือคะแนนในอุดมคติของ IEF ในขณะที่ค่า IEF ที่มากกว่า 10.13 คือคะแนนที่สามารถบ่งบอกถึงความจำเป็นในการพิจารณาใช้การจัดการเรื่องการหายใจ อย่างไรก็ตามในกรณีที่มีการคำนวณค่า IEF แล้วได้รับคะแนนต่ำกว่า 10.13 จำเป็นจะต้องตรวจสอบลักษณะการเคลื่อนที่ของก้อนมะเร็งอีกครั้ง หากการเคลื่อนที่ของก้อนมะเร็งด้านใดด้านหนึ่งเกิน 5 มิลลิเมตร ผู้ป่วยรายนั้นจะต้องได้รับพิจารณาใช้การจัดการเรื่องการหายใจรูปแบบใดรูปแบบหนึ่ง

สาขาวิชา           ฟิสิกส์การแพทย์  
ปีการศึกษา        2564

ลายมือชื่อนิติศ .....  
ลายมือชื่อ อ.ที่ปรึกษาหลัก .....

## 6174754530 : MAJOR MEDICAL PHYSICS

KEYWORD: Interplay effects, SBRT, VMAT, Lung cancer

Vanida Poolnapol : Dosimetric impact of interplay effects in Stereotactic Body Radiation Therapy (SBRT) lung cancer. Advisor: Asst. Prof. TAWEAP SANGHANGTHUM, Ph.D.

Lung cancer patient breathing induced interplay effects in the volumetric modulated arc therapy (VMAT) together with stereotactic body radiation therapy (SBRT), which lead to non-uniform doses within the target volume and unwanted dose to the surrounding tissues. The purpose of this study was to investigate the dosimetric impact of interplay effects in 6 MV FFF of photon beams for lung cancer and to calculate the novel interplay effects factor (IEF) for VMAT-SBRT lung cancer. This study performed the static and dynamic measurements using two dimensions (2D) robotic platform and diode array for 3D-conformal radiation therapy (3D-CRT) plans, while using three dimensions (3D) CIRS dynamic thorax phantom and EBT3 films, and CC01 ionization chambers for VMAT-SBRT plans. The 3D-CRT results, the 1%, 1mm of gamma passing rates decreased for higher amplitudes. However, gamma passing rates increased with larger field sizes. For other parameters, no interplay effect was detected. The VMAT-SBRT results showed that higher amplitudes, more dimensions, and smaller doses are more pronounced. Therefore, the IEF calculation parameters consisted of these three mentioned factors. The 10.13 was the suitable number to be used as the cut point of lung VMAT-SBRT for applying respiratory motion management. The interplay effects for 6 MV FFF photon beams in VMAT-SBRT lung cancer are more impacted for the higher amplitudes and dimensions, and the smaller doses. The breathing amplitudes above 5 mm lead to significant changes in the shape of dose distribution due to the interplay effects, especially for 3D movements. The novel interplay effects factor (IEF) is a parameter that can indicate the interplay effects directly for VMAT-SBRT lung cancer patients. The value of 1 is the ideal score of IEF, while a value more than 10.13 is the score that can imply the need of respiratory motion management. However, the score is lower than 10.13, but that case provides some tumor motion that exceeds 5 mm in all directions, the need for respiratory motion management was also recommended.

Field of Study: Medical Physics

Student's Signature .....

Academic Year: 2021

Advisor's Signature .....

## ACKNOWLEDGEMENTS

I would like to offer my heartfelt thanks to Assistant Professor Taweap Sanghangthum, Ph.D. Department of Radiology, Faculty of Medicine, Chulalongkorn University, and Mintra Keawsamur, Ph.D. Division of Radiation Oncology, Department of Radiology, King Chulalongkorn Memorial Hospital, my advisor and co-advisor for their instructions, supports, care and polishing the research work to its final version.

I am also thankful to Associate Professor Sivalee Suriyapee, Department of Radiology, Faculty of Medicine, Chulalongkorn University, my teacher for her instruction, support and constructive advice in the research.

I am grateful to Associate Professor Anchali Krisanachinda, Ph.D. Division of Nuclear Medicine, Department of Radiology, Faculty of Medicine, Chulalongkorn University, who was the chairman of the dissertation defense for her suggestion and comments in this research.

I greatly appreciate Sornjarod Oonsiri, Ph.D. Department of Radiology, Faculty of Medicine, Chulalongkorn University, and all physicists at Radiotherapy Center, Department of Oncology, King Chulalongkorn Memorial Hospital for a very kind suggestion and instruction.

My sincere thank is passed to Assistant Professor Danita Kannarunimit, M.D. and Anussara Prayongrat, M.D., Ph.D. Division of Radiation Oncology, Department of Radiology, King Chulalongkorn Memorial Hospital, her kindness suggestion and comments in this research.

Also, my thank is offered to Professor Franco Milano, Ph.D. who is the external examiner of the thesis, for his help, kind suggestion and comments for this research.

My heartfelt thank is passed to all cancer patients for keeping my motivation to complete this dissertation.

Finally, I would like to greatly thank to my family for their encouragement and everything they have done to my life.

Vanida Poolnapol

## TABLE OF CONTENTS

	<b>Page</b>
ABSTRACT (THAI).....	iii
ABSTRACT (ENGLISH).....	iv
ACKNOWLEDGEMENTS.....	v
TABLE OF CONTENTS.....	vi
LIST OF TABLES.....	vi
LIST OF FIGURES.....	vi
LIST OF ABBREVIATIONS.....	vi
CHAPTER 1.....	1
BACKGROUND AND RATIONALE.....	1
1.1 Background and rationale.....	1
1.2 Research objectives.....	3
1.2.1 Primary objective.....	3
1.2.2 Secondary objective.....	3
CHAPTER 2.....	4
REVIEW OF RELATED LITERATURES.....	4
2.1 Theories.....	4
2.1.1 Lung carcinoma.....	4
2.1.1.1 The incidence of lung carcinoma.....	4
2.1.1.2 Treatment of choice for lung carcinoma.....	5
2.1.1.3 Stereotactic body radiation therapy (SBRT).....	5
2.1.2 Planning techniques.....	7

2.1.2.1 3D-conformal radiation therapy (3D-CRT).....	7
2.1.2.2 Intensity-modulated radiotherapy (IMRT) .....	8
2.1.2.3 Volumetric modulated arc therapy (VMAT).....	9
2.1.3 Breathing cycle.....	10
2.1.4 Interplay effects.....	11
2.1.5 Detectors .....	12
2.1.5.1 Semiconductor detector .....	12
2.1.5.2 GafChromic EBT3 film (27).....	13
2.1.5.3 Ionization chamber.....	14
2.1.6 Plan evaluation.....	15
2.1.6.1 The percent point dose difference.....	16
2.1.6.2 Gamma evaluation method.....	16
2.2 Related works.....	18
CHAPTER 3 .....	20
RESEARCH METHODOLOGY.....	20
3.1 Research design.....	20
3.2 Research design model.....	20
3.3 Conceptual framework.....	20
3.4 Keywords .....	21
3.5 Research questions.....	21
3.5.1 Primary question: .....	21
3.5.2 Secondary question .....	21
3.6 Materials information.....	21
3.6.1 CT simulator (30).....	22



3.6.2 Lung patient images .....	23
3.6.3 Treatment planning system and dose calculation algorithm .....	23
3.6.4 TrueBeam linear accelerator .....	23
3.6.5 Phantoms .....	24
3.6.5.1 MotionsSimXY/4D dynamic phantom .....	24
3.6.5.2 Solid water phantom .....	25
3.6.5.3 CIRS dynamic thorax phantom model 008A.....	25
3.6.6 Detectors .....	27
3.6.6.1 MapCHECK2 2D diode array.....	27
3.6.6.2 Gafchromic EBT3 film .....	28
3.6.6.3 Film scanner.....	28
3.6.6.4 CC01 ionization chamber .....	29
3.6.6.5 Dose1 electrometer .....	30
3.7 Methods.....	30
3.7.1 Actual tumor motion collection .....	31
3.7.2 Experimental design part1.....	31
3.7.2.1 Planning preparation part1 .....	31
3.7.2.2 Dose measurement part1 .....	32
3.7.3 Experimental design part2.....	33
3.7.3.1 Film calibration.....	33
3.7.3.2 CIRS phantom CT-scanning.....	34
3.7.3.3 Planning preparation part2.....	35
3.7.3.4 Dose measurement part2.....	36
3.7.4 Novel interplay effects factor (IEF) calculation.....	38

3.8 Outcome measurement.....	39
3.8.1 Part of dose measurements.....	39
3.8.2 Part of novel interplay effects factor calculation .....	39
3.9 Expected benefits .....	39
3.9.1 Primary benefit.....	39
3.9.2 Secondary benefit.....	39
3.10 Ethical consideration.....	39
CHAPTER 4 .....	41
RESULTS .....	41
4.1 Actual tumor motion collection .....	41
4.2 Experiment part1 .....	42
4.2.1 Amplitude test.....	42
4.2.2 Phase test.....	44
4.2.3 Field sizes test.....	45
4.2.4 Dose test.....	46
4.2.5 Dose rate test.....	46
4.2.6 No. of fraction test.....	47
4.3 Experiment part2.....	47
4.3.1 Film calibration.....	47
4.3.2 1D amplitude tests.....	48
4.3.3 2D amplitude tests.....	51
4.3.4 3D amplitude tests.....	55
4.3.5 Phase test.....	56
4.3.6 Tumor size test.....	57

4.3.7 Dose test.....	57
4.3.8 Dose rate test.....	59
4.3.9 No. of fraction test.....	59
4.3.10 No. of arc test.....	60
4.3.11 Plan complexity (MU/Gy).....	61
4.4 Novel interplay effects factor (IEF) calculation.....	61
CHAPTER 5 .....	64
DISCUSSION AND CONCLUSIONS .....	64
5.1 Discussion of experiment part1.....	64
5.2 Discussion of experiment part2.....	65
5.3 Discussion of novel IEF calculation .....	67
Conclusions .....	68
REFERENCES.....	69
APPENDIX.....	72
.....	72
VITA .....	73

## LIST OF TABLES

	<b>Page</b>
Table 2. 1 Global cancer incidence of new cases and deaths in 2020. ....	4
Table 2. 2 Lung tumor–motion data. The mean range of motion and the (minimum–maximum). 19	19
Table 3. 1 Characteristics of the CIRS dynamic thorax phantom components. ....	26
Table 3. 2 The 3D-CRT planning parameters.....	32
Table 3. 3 All parameters setting of dosimetric measurement part1. ....	33
Table 3. 4 The VMAT-SBRT planning parameters.....	36
Table 3. 5 All parameters setting of amplitude tests in dose measurement part2.....	37
Table 3. 6 All parameters setting of phase, dose rate, no. of arc, tumor size, dose, no. of fraction, and plan complexity tests in dose measurement part2.....	38
Table 4. 1 The longest distance of actual tumor motion in each direction of 9 lung cancer patients who underwent SBRT treatment technique. ....	41
Table 4. 2 The gamma passing rates of 1%, 1mm criteria of 3D-CRT plans irradiation with different amplitudes and unpaired t-test statistical analysis between 1D (X or Y-axis) and 2D (XY-axis) moving patterns.....	42
Table 4. 3 The gamma passing rates of 1%, 1mm criteria of 3D-CRT plans irradiation with different phases. ....	44
Table 4. 4 The gamma passing rates of 1%, 1mm criteria of 3D-CRT plans irradiation with different field sizes.....	45
Table 4. 5 The gamma passing rates of 1%, 1mm criteria of 3D-CRT plans irradiation with different doses.....	46

Table 4. 6 The gamma passing rates of 1%, 1mm criteria of 3D-CRT plans irradiation with different dose rates. ....	46
Table 4. 7 The gamma passing rates of 1%, 1mm criteria of 3D-CRT plans irradiation with different no. of fractions.....	47
Table 4. 8 The gamma passing rates of 3%, 2mm criteria of VMAT-SBRT irradiation with different 1D amplitudes of X-axis. ....	48
Table 4. 9 The gamma passing rates of 3%, 2mm criteria of VMAT-SBRT irradiation with different 1D amplitudes of Y-axis. ....	49
Table 4. 10 The gamma passing rates of 3%, 2mm criteria of VMAT-SBRT irradiation with different 1D amplitudes of Z-axis.....	49
Table 4. 11 The gamma passing rates of 3%, 2mm criteria of VMAT-SBRT irradiation with different 2D amplitudes of XY-axis.....	52
Table 4. 12 The gamma passing rates of 3%, 2mm criteria of VMAT-SBRT irradiation with different 2D amplitudes of XZ-axis.....	52
Table 4. 13 The gamma passing rates of 3%, 2mm criteria of VMAT-SBRT irradiation with different 2D amplitudes of YZ-axis.....	53
Table 4. 14 The gamma passing rates of 3%, 2mm criteria of VMAT-SBRT irradiation with different 3D amplitudes of XYZ-axis.....	55
Table 4. 15 The gamma passing rates of 3%, 2mm criteria of VMAT-SBRT plans irradiation with different phases. ....	56
Table 4. 16 The gamma passing rates of 3%, 2mm criteria of VMAT-SBRT plans irradiation with different tumor sizes.....	57
Table 4. 17 The gamma passing rates of 3%, 2mm criteria of VMAT-SBRT plans irradiation with different doses.....	58

Table 4. 18 The gamma passing rates of VMAT-SBRT planned irradiation with different dose rates of 3%, 2mm. ....	59
Table 4. 19 The gamma passing rates of VMAT-SBRT planned irradiation with different fractions at 3%, 2mm. ....	60
Table 4. 20 The gamma passing rates of 3%, 2mm criteria of VMAT-SBRT plans irradiation with different numbers of arcs. ....	60
Table 4. 21 The gamma passing rates of 3%, 2mm criteria of VMAT-SBRT plans irradiation with different plan complexity. ....	61
Table 4. 22 The scaling of score for tumor motion dimension parameter. ....	62
Table 4. 23 The scaling of score for breathing amplitude parameters. ....	62
Table 4. 24 The clinical information and the IEF score of 29 lung SBRT patients were applied. .	63

## LIST OF FIGURES

	<b>Page</b>
Figure 2. 1 The isodose distribution of lung cancer patient who underwent VMAT-SBRT planning technique.....	5
Figure 2. 2 Schematic volume of target and critical structure definition reported by ICRU Reports No. 50 and 62.....	7
Figure 2. 3 The left lung cancer with 3D-CRT planning treatment technique. ....	8
Figure 2. 4 The left lung cancer with VMAT planning treatment technique.....	10
Figure 2. 5 (A) The simulation of the patient's respiratory cycle consists of: amplitude, phase, inhalation range, and exhalation range. (B) The mechanism of breathing involves two main processes: inhalation and exhalation.....	11
Figure 2. 6 Interplay effects diagram. The incongruous of tumor and MLC motion conduct inhomogeneous inside the tumor and/or unwanted dose to the surrounding tissue in (B) a real situation compare to (A) an ideal situation. ....	12
Figure 2. 7 Schematic diagram of Semiconductor diode detector. ....	12
Figure 2. 8 The solid-state polymerization of GafChromic film. ....	14
Figure 2. 9 Structure of GafChromic EBT3 dosimetry film. ....	14
Figure 2. 10 Schematic diagram of the simplest of all gas-filled radiation detector. ....	15
Figure 2. 11 The geometric representation of dose distribution evaluation criteria using the combined ellipsoidal dose-difference and distance-to-agreement tests. ....	17
Figure 3. 1 Research design model. ....	20
Figure 3. 2 Conceptual frameworks.....	21

Figure 3. 3 The Philips Brilliance Big Bore CT scanner. ....	22
Figure 3. 4 The Eclipse™ Treatment Planning System. ....	23
Figure 3. 5 The TrueBeam millennium 120 MLC linear accelerator. ....	24
Figure 3. 6 The MotionsSimXY/4D dynamic phantom with the MapCHECK2.....	25
Figure 3. 7 The CIRS model 008A dynamic thorax phantom. ....	26
Figure 3. 8 The SBRT insert with 1, 2, and 3 cm diameter of soft-tissue equivalent targets. ....	26
Figure 3. 9 The microchamber insert with 1, 2, and 3 cm diameter of soft-tissue equivalent targets. .....	27
Figure 3. 10 The SNC patient software.....	28
Figure 3. 11 The Gafchromic EBT3 self-developing dosimetry film.....	28
Figure 3. 12 The Epson Perfection V700 Photo film scanner. ....	29
Figure 3. 13 The CC01 ionization chamber.....	29
Figure 3. 14 The Dose1 electrometer.....	30
Figure 3. 15 The setting up of the MotionSimXY/4D dynamic phantom, the MapCHECK2, and the solid water phantom.....	32
Figure 3. 16 Film calibration setting up on the solid water phantom. ....	34
Figure 3. 17 The CT images of CIRS dynamic thorax phantom with CC01 dosimeter and 2 cm diameter of microchamber insert in 0, -45, and -90° degrees.....	35
Figure 3. 18 The certificate of approval from ethic committee of the Faculty of Medicine Chulalongkorn University.....	40



Figure 4. 1 The correlation curves of 1D moving patterns between the gamma passing rates and the different X amplitudes. ....	43
Figure 4. 2 The correlation curves of 1D moving patterns between the gamma passing rates and the different Y amplitudes. ....	43
Figure 4. 3 The correlation curves of 2D moving patterns between the gamma passing rates and the different XY amplitudes.....	44
Figure 4. 4 The correlation curves of 2D moving patterns between the gamma passing rates and the different field sizes.....	45
Figure 4. 5 The film calibration curve between absorbed dose and pixel value.....	48
Figure 4. 6 The correlation curves of 1D moving patterns between the gamma passing rates and the different X amplitudes. ....	50
Figure 4. 7 The correlation curves of 1D moving patterns between the gamma passing rates and the different Y amplitudes. ....	50
Figure 4. 8 The correlation curves of 1D moving patterns between the gamma passing rates and the different Z amplitudes.....	51
Figure 4. 9 The correlation curves of 2D moving patterns between the gamma passing rates and the different XY amplitudes.....	53
Figure 4. 10 The correlation curves of 2D moving patterns between the gamma passing rates and the different XZ amplitudes. ....	54
Figure 4. 11 The correlation curves of 2D moving patterns between the gamma passing rates and the different YZ amplitudes. ....	54
Figure 4. 12 The correlation curves of 3D moving patterns between the gamma passing rates and the different XYZ amplitudes. ....	56

Figure 4. 13 The correlation curves of 3D moving patterns between the gamma passing rates and the different dose.....58

Figure A. 1 The linear correlation between signal (nC) and MU of linearity test of CC01. ....72



## LIST OF ABBREVIATIONS

2D	Two-dimensional
3D	Three-dimensional
3D-CRT	Three-dimensional conformal radiation therapy
4DCT	Four-dimensional computed tomography
AAA	Analytical anisotropic algorithm
AAPM	American association of physicists in medicine
Amp	Amplitude
AP	Anteroposterior
BED	Biologically equivalent dose
BT	Brachytherapy
CA	Cancer
CIRS	Computerized imaging reference system
CT	Computed tomography
CTV	Clinical target volume
DD	Dose difference
dpi	dots per inch
DTA	Distance to agreement
DVH	Dose volume histogram
FF	Flattening filter
FFF	Flattening filter free
GTV	Gross tumor volume
Gy	Gray
IC	Ionization chamber
ICRU	International commission on radiation units and measurements
IEF	Interplay effect factor
IMRT	Intensity modulated radiotherapy
IMPT	Intensity modulated proton therapy
ITV	Internal target volume

IVS	Interplay effect variable score
keV	Kilo electronvolt
LR	Left-right
MCSv	Modulation complexity score for VMAT
MLC	Multi-leaf collimator
min	Minute
MIP	Maximum intensity projection
MRI	Magnetic resonance imaging
MU	Monitor units
MV	Megavolt
NBs	Number of breaths
NSCLC	Non-small cell lung cancer
OARs	Organs at risk
PTV	Planning target volume
QA	Quality assurance
R <sup>2</sup>	R-squared value
ROI	Region of interest
RPM	Real-time position management
SAD	Source-axis distance
SBRT	Stereotactic body radiation therapy
SCLC	Small cell lung cancer
sec	Second
SFOV	Scan field of view
SI	Supero-inferior
SNC	Sun nuclear corporation
SRS	Stereotactic radiosurgery
TMMCSv	The combination of tumor motion and MCSv
TPS	Treatment planning system
VMAT	Volumetric modulated arc therapy

## CHAPTER 1

### BACKGROUND AND RATIONALE

#### 1.1 Background and rationale

Lung cancer is the second most common malignancy in both genders worldwide. Also, it is the leading cause of death worldwide, accounting for an estimated 1.80 million cases in 2020 (1). One of the most common lung irradiation treatment techniques is stereotactic body radiation therapy (SBRT).

SBRT is a cancer treatment technique that delivers extremely precise, very intense doses of radiation to cancer cells while minimizing damage to healthy tissue. As the treatment involves large doses in few fractions together with a rapid fall-off of dose outside the target volume, the accuracy of dose delivery and conformity of dose are very essential. Tsang MW (2) insisted that this special technique has emerged as the standard treatment for medically inoperable early-stage non-small cell lung cancer (NSCLC). The local control rate after SBRT is over 90%, while the tumor target can achieve a high radiation dose without overdose at surrounding normal tissues. Therefore, SBRT has been widely adopted for the treatment of oligo-metastasis involving the lung, as well as its potential applications in a variety of other cancers, in addition to medically inoperable stage I NSCLC. In addition, John C et al. (3) revealed the SBRT technique has evolved into an effective and safe treatment modality for both primary and secondary pulmonary malignancies. However, this technique still poses a challenge to the treatment of lung cancer due to the interplay effects during radiation treatment.

The interplay effects are the dynamic interactions between tumor motion owing to patient breathing and multi-leaf collimator (MLC) motion that occurs at the same time. These simultaneous motions, which lead to heterogeneities within the target volume and/or an unwanted dose to the surrounding tissue, must be concerned. A previous study by Pawiro SA et al. (4) indicated that the tumor motion during irradiation could bring dose validation inside the tumor target in both lung intensity modulated radiation therapy (IMRT) and volumetric modulated arc therapy (VMAT) treatment techniques. Likewise, a study by Adamczyk M et al. (5) illustrated that the lung three-dimensional conformal radiotherapy (3D-CRT) and IMRT treatment techniques could cause

tumors under dosage due to the interplay effect. Furthermore, several studies (6) (7) (8) (9) revealed that the dose distribution of the tumor target was blurred during irradiation as a result of the interplay effects.

In recent years, the flattening filter free (FFF) technique has been utilized together with the SBRT technique to increase the efficiency of lung cancer treatment (10) (11) and reduce the interplay effects (7). It has several benefits, such as providing a higher dose rate with shorter treatment time as well as allowing inhomogeneous dose distribution with reduced peripheral dose (12) (13) (14). Although the combined techniques can relieve the interplay effects, many factors still impact these interplay effects.

A study by Edvardsson A et al. (7) demonstrated that the interplay effects of VMAT radiotherapy are affected by many parameters such as breathing pattern, plan complexity, dose, dose rate, clinical target volume (CTV) size, and multiple fractions. A study by Kubo K et al. (15) revealed the number of breaths (NBs) is another important parameter to reduce the dose variation caused by the interplay effect with VMAT-SBRT for lung cancer. Additionally, this paper also showed various interesting parameters i.e. the interplay effect variable score (IVS). The IVS is calculated by four factors: the product of the combination of tumor motion (TMMCSv), modulation complexity score for VMAT (MCSv) (16) (17), NBs, and amplitude of tumor in SI direction. The studies mentioned above represented various types of parameters that affect the interplay effects during irradiation. Nonetheless, nothing can accurately represent the interactions of VMAT-SBRT lung cancer. Furthermore, all studies considered only one direction of tumor motion. A report of the American Association of Physicists in Medicine (AAPM) task group number 76 (18) illustrates that the lung tumor does not move only in the SI direction.

Consequently, the research intends to apply the strengths of the FFF technique to study the impact of interplay effects by varying dosimetric parameters of amplitude, phase, field size, dose, dose rate, number of fractions, number of arcs, tumor size, and plan complexity, which can produce the interplay effects during lung SBRT irradiation. Furthermore, the study is aimed to develop a novel interplay effect factor (IEF) which can directly refer to the interplay effects of VMAT-SBRT lung cancer.

## **1.2 Research objectives**

### **1.2.1 Primary objective**

To investigate the impact of the dosimetric parameters of interplay effects in 6 MV FFF photon beams for lung cancer.

### **1.2.2 Secondary objective**

To calculate the novel IEF for VMAT-SBRT lung cancer.



## CHAPTER 2

### REVIEW OF RELATED LITERATURES

#### 2.1 Theories

##### 2.1.1 Lung carcinoma

Lung cancer is a type of cancer that originates in the lungs. Cancer develops when cells in the body begin to grow out of control. There are two main types of lung cancer, namely: non-small cell lung cancer (NSCLC) and small cell lung cancer (SCLC). About 80% to 85% are NSCLC while, about 10% to 15% are SCLC; fewer than 5% are other types of lung tumors such as cancers that metastasize from other organs (e.g. breast, pancreas, kidney, or skin) (19).

##### 2.1.1.1 The incidence of lung carcinoma

Lung cancers were the second most commonly diagnosed cancer worldwide, each contributing 11.4% of the total number of new cases diagnosed in 2020. It is the leading cause of the highest death worldwide, an estimated 1.80 million cases in 2020 (1) as shown in table 2.1.

Table 2. 1 Global cancer incidence of new cases and deaths in 2020.

Rank	Cancer sites	No. of new cases	No. of deaths
	All cancers*	19,292,789	9,958,133
1	Female breast	2,261,419	684,996
2	Lung	2,206,771	1,796,144
3	Prostate	1,414,259	375,304
4	Nonmelanoma	1,198,073	63,731
5	Colon	1,148,515	576,858



### 2.1.1.2 Treatment of choice for lung carcinoma

There are four main choices for lung carcinoma treatment, namely: surgery, chemotherapy, targeted therapy, and radiotherapy. One of the most common lung irradiation techniques is the SBRT treatment technique used in small target cases.

### 2.1.1.3 Stereotactic body radiation therapy (SBRT)

SBRT refers to a stereotactic radiotherapy procedure for treating extracranial tumors with ultra-high doses per fraction, in few fractions. SBRT has been mostly applied to tumors in the spine, lung, liver, pancreas, kidney, and prostate (20). Because SBRT delivers large doses in few fractions to the target together with the rapid fall-off of dose outside the target, it is critically important to minimize damage to normal tissue, as shown in figure 2.1. Thus, the accuracy of dose delivery and conformity of dose is very important.

SBRT's main characteristics include: 1. a high dose in a small number of fractions; 2. extracranial tumors with a maximum diameter of about 5 centimeters (cm) or less; 3. a few millimeters (mm) margins or none (9); 4. stringent need for patient immobilization; 5) respiratory motion management request.

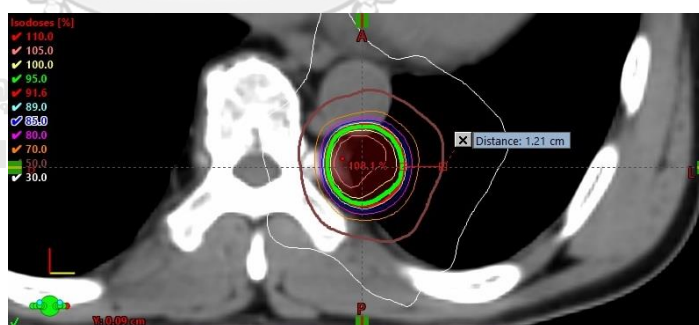


Figure 2. 1 The isodose distribution of lung cancer patient who underwent VMAT-SBRT planning technique.

For SBRT simulation, sufficient patient immobilization, management of tumor motion, and three dimensions (3D) image acquisition for treatment planning and image-guided treatment delivery are necessary.

Patient immobilization: Since the high doses of delivery were required, conventional immobilization devices were inadequate to ensure accurate and reproducible patient fixation. Thus, the special immobilization devices were applied for SBRT cases. As a result, the stereotactic body frames can improve patient reproducibility to within a couple of millimeters. The abdominal compression devices, such as the manual or pneumatic compression belt, induce shallow breathing and thus minimize respiratory motion. However, variations in the position of the target can be larger due to intrafraction internal target motion.

Tumor motion management: Tumor motion management can be divided into two main parts: passive and active motion management strategies. Passive motion management involves accounting for target volume delineation from four-dimensional computed tomography (4DCT) datasets which correspond to different phases of the respiratory cycle. For 4DCT images of lung cancer, the maximum intensity projection (MIP) image is useful in determining the full extent of tumor motion throughout all phases of the respiratory cycle. The average intensity projection image is the mean intensity of the patient at each voxel. These images are typically used for the determination of the internal target volume (ITV) for treatment planning. Active motion management involves either reducing the amount of tumor motion during treatment for example, via real-time tracking or respiratory gating techniques to account for the tumor motion, or deep inspiration/expiration breath-hold techniques that are sometimes employed to reduce the amount of tumor motion during respiration.

3D image acquisition: Computed tomography (CT) images are the gold standard for target volumes and organs at risk (OARs) delineation. The slice thickness should be sufficiently small ( $\leq 3$  mm) to allow for accurate contouring of all structures. In the SBRT planning, the target volume was defined following the ICRU 50 and ICRU 62 reports (21) (22). There is gross tumor volume (GTV), clinical target volume (CTV), and internal target volume (ITV), which is the CTV plus an internal margin. This internal margin is designed to take into account the variations in the size and position of the CTV relative to the patient's reference frame as displayed in figure

2.2. The variations are due to organ motions such as breathing and bladder or rectal contents (22). In addition, the AAPM TG 101 report (23) recommends the use of an anisotropic grid spacing of 2 mm or less for the SBRT dose calculation step. For dose calculation algorithms, they should be capable of determining doses near the lung-tissue interfaces due to lateral electron scattering of heterogeneous tissue, such as convolution-superposition or Monte Carlo.

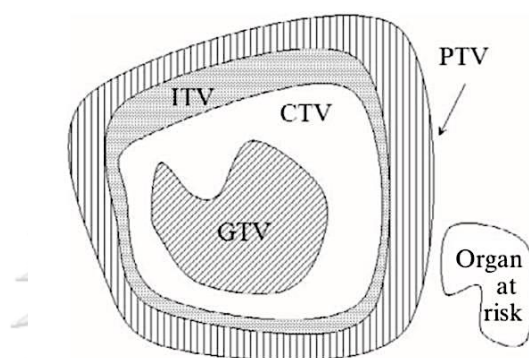


Figure 2. 2 Schematic volume of target and critical structure definition reported by ICRU Reports No. 50 and 62.

The biological effects of the SBRT treatment technique are larger than with conventional fractionation, owing to the giving of an ultrahigh dose in a few irradiation times. To represent the biological effects of SBRT, the biologically equivalent dose (BED) calculation should be applied. Moreover, the quality assurance for SBRT must be performed before treatment following the AAPM TG-142 report (24).

## 2.1.2 Planning techniques

### 2.1.2.1 3D-conformal radiation therapy (3D-CRT)

3D-CRT is a radiation therapy technique that can view a tumor in three dimensions with the help of image guidance. Therefore, this technique can deliver radiation beams from several directions to the tumor and is able to conform the radiation beams to the shape of a tumor using the MLC for modern radiotherapy machines while limiting radiation exposure to the surrounding healthy tissues. Higher

beam energies are more regarded for the thickness of a patient's body part to increase the dose to the center and reduce the dose to the skin as well as subcutaneous tissues. 3D-CRT is a forward treatment planning system where the user designs the plans into a radiotherapy treatment planning system. The required decisions include beam energy, number of beams, beam directions, and prescription dose. In order to receive conformal treatment, the beam weighting, wedges, electronic tissue compensators, and other parameters need to be adjusted. The dose volume histogram (DVH) and tolerance limit of each OAR is used for planning evaluation. The strength of this technique is the giving of homogeneous doses within irradiation fields and the use of short treatment periods. For lung cancer, the 3D-CRT technique has been considered as the common treatment choice in lung irradiation treatment. Figure 2.3 shows the combination of multiple uniform radiation doses to deliver precise doses of radiation to the lung tumor.

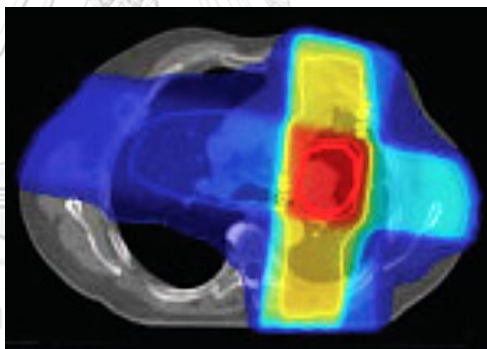


Figure 2. 3 The left lung cancer with 3D-CRT planning treatment technique.

#### 2.1.2.2 Intensity-modulated radiotherapy (IMRT)

IMRT is the technique that can create more conformal dose distribution to the target volume compared to 3D-CRT planning technique. IMRT is capable of achieving better sparing of surrounding normal tissues with the use of multiple optimized beams from different directions to create non-uniform dose distributions using MLC movement to modulate the beam. However, this technique has several weaknesses. First, it gives approximately 10 times higher monitor units than 3D-CRT technique, which raises a concern about leakage radiation, secondary malignancy,

and neutron contamination, especially for high energy photon beams. Second, it takes relatively longer treatment time, which can increase the chances of patient movement during beam delivery that might affect the treatment outcome. Furthermore, IMRT is the inverse treatment planning. In contrast to the manual trial-and-error process of forward planning, the inverse planning uses the optimizer to solve the inverse problem as set by the planner. In inverse planning, radiation oncologist defines a patient's critical organs and tumor. Afterward, the planner sets target doses for both tumors and organs at risk. Then, an optimization program is run to find the treatment plan which best matches all the input criteria. Inverse planning uses the optimizer to solve the inverse problem as has been set by the planner.

#### **2.1.2.3 Volumetric modulated arc therapy (VMAT)**

VMAT is the technique that can create more conformal dose distribution to the target volume compared to the 3D-CRT planning technique. This technique is capable of achieving better sparing of the surrounding normal tissues with the use of multiple optimal arcs of beams from different degrees to create non-uniform dose distributions using MLC movement to modulate the beam (figure 2.4). VMAT delivers a precisely sculpted 3D dose distribution during gantry rotation. The machine continuously re-shapes and changes the intensity of the radiation beam as it moves around the patient with three modulating parameters: MLC, dose rate, and gantry speed. In addition, VMAT allows lower monitor unit (MU) closely to 3D-CRT planning technique. For planning, VMAT is an inverse planning technique that sets up the dose constraints by the planner according to tolerance organ limits protocol. The result of dose distribution in the VMAT planning technique is slightly similar to the IMRT planning technique which provides the conformity of radiation dose to the target volume, while can spare the surrounding OARs. Nevertheless, VMAT uses the continuous rotation gantry to give the radiation dose. Hence, the low doses outside the target are higher than the IMRT along with the small size or spherical shape of tumors are more suitable to deal with this technique example for stereotactic radiosurgery (SRS), stereotactic radiotherapy (SRT), or SBRT cases. Figure 2.4

shows two half arc planning techniques, which provides non-uniform doses in treatment fields, to the tumor in left lung.

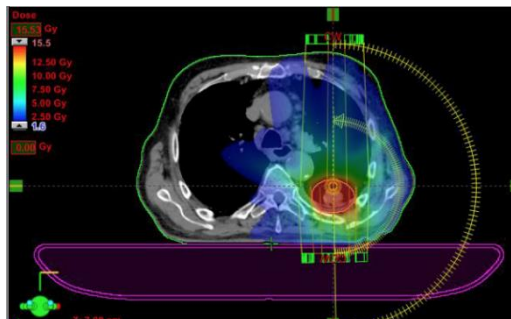


Figure 2. 4 The left lung cancer with VMAT planning treatment technique.

### 2.1.3 Breathing cycle

The breathing cycle is a description of the changes in pressure, lung volume, and airflow that occur during a single cycle of breathing (25). The breathing cycle in figure 2.5 (A) can be divided into two basic parts, including amplitude and phase. The amplitude depth of breathing while the phase is the time of the respiratory cycle. The increasing range of amplitude is called inspiration. In the opposite direction, the decreasing range of amplitude is called expiration. Inspiration occurs when lung pressure is decreased below the atmospheric pressure that causes the air to flow into the lungs. During inspiration, the diaphragm contracts and pulls downward while the muscles between the ribs contract and pull upward. On the other hand, expiration occurs when the lung pressure is increased above the atmospheric pressure, and that pushes the air out of the lungs. During expiration, the diaphragm relaxes and the volume of the thoracic cavity decreases, while the pressure within it increases. As a result, the lungs contract and air is forced out, as illustrated in figure 2.5 (B).

As for lung cancer, the tumor motion owing to patient breathing becomes a significant problem during radiation treatment. Therefore, respiratory motion management has been applied to reduce the dose validation due to the interplay effects during irradiation. In lung CA clinical treatment, managing respiratory motion in radiotherapy has an abundance of techniques which have been mentioned above in tumor motion management part.

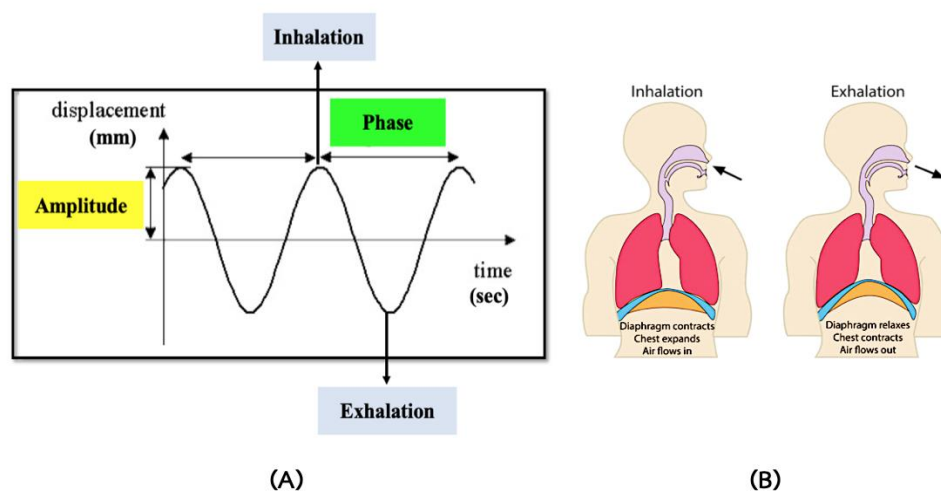


Figure 2. 5 (A) The simulation of the patient's respiratory cycle consists of: amplitude, phase, inhalation range, and exhalation range. (B) The mechanism of breathing involves two main processes: inhalation and exhalation.

#### 2.1.4 Interplay effects

Interplay effects are the effects between tumor motion and MLC motion that occur at the same time. This affects both dose delivery accuracy and dose conformity during lung cancer treatment. As a result, treatment techniques that produce steep dose gradients, such as SRS, SRT, SBRT, or intensity-modulated proton therapy (IMPT), must be considered. As the high dose gradients are planned for the target volume and the normal tissue, thus when the target moves, interplay will result in heterogeneities doses within the target volume and/or unwanted doses to the surrounding tissue in comparison with the static treatment plan as shown in figure 2.6.

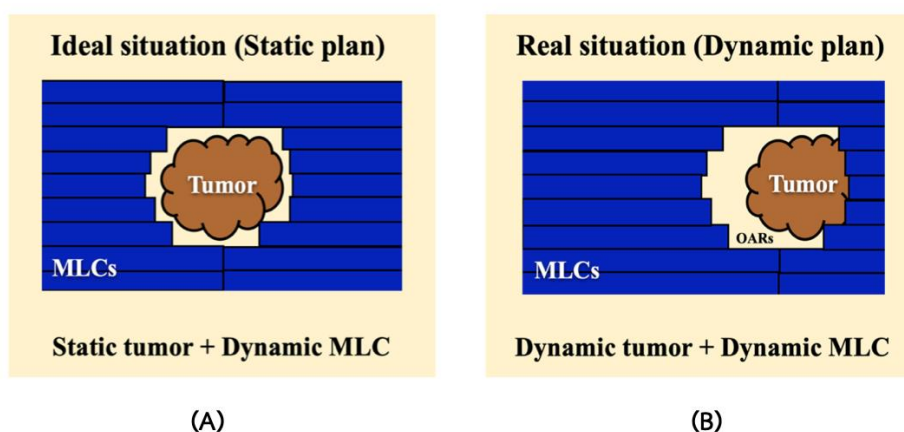


Figure 2. 6 Interplay effects diagram. The incongruous of tumor and MLC motion conduct inhomogeneous inside the tumor and/or unwanted dose to the surrounding tissue in (B) a real situation compare to (A) an ideal situation.

## 2.1.5 Detectors

### 2.1.5.1 Semiconductor detector

Semiconductor diode detectors act as solid state on application of a reverse bias to the detectors and on the exposure to radiation. The sensitivity of solid state detectors are higher than gas filled detectors, owing to the lower average energy required to produce an ion pair in solid detector materials compared with air and the higher density of the solid detector materials compared with air.

Operation of a diode, the device consists of a p-n junction across which a pulse of current develops when a particle of ionizing radiation traverses it. In a different device, the absorption of ionizing radiation generates pairs of charge carriers (electrons and holes) in a block of semiconducting material; the migration of these carriers under the influence of a voltage maintained between the opposite faces of the block constitutes a pulse of current. The pulses created in this way are amplified, recorded, and analyzed to determine the energy, number, or identity of the incident-charged particles (26). The diagram of solid-state detector is shown in figure 2.7.

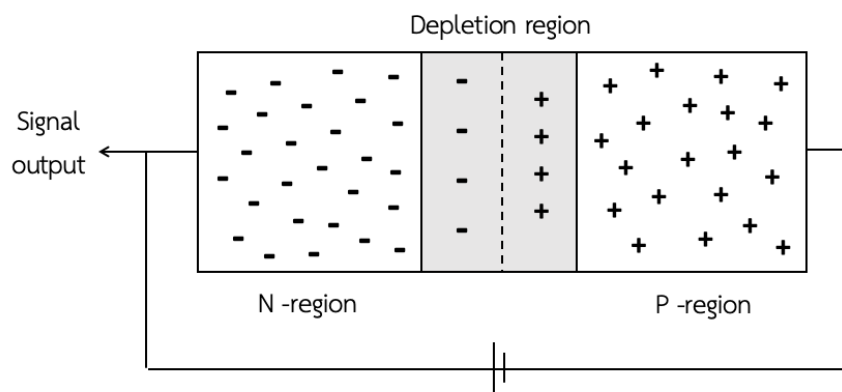


Figure 2. 7 Schematic diagram of Semiconductor diode detector.



### 2.1.5.2 GafChromic EBT3 film (27)

The EBT3 film is the self-developing dosimetry film that involves the direct coloration of a material by the absorption of energetic radiation, without requiring latent chemical or thermal development. The radiochromic reaction is a solid-state polymerization, whereby the films turn deep blue proportionately to the radiation dose, due to progressive 1,4-trans additions which lead to colored polyconjugated, ladderlike polymer chains as shown in figure 2.8. The EBT3 film was designed for the measurement of absorbed dose of ionizing radiation. It is particularly suited for high energy photon. The dynamic range of this film is designed for the best performance in the dose range from 0.2 to 10 Gy, making it suitable for many applications in IMRT, VMAT and brachytherapy.

The structure of the EBT3 film is shown in figure 2.9. The film is comprised of an active layer, nominally 28  $\mu\text{m}$  thick, sandwiched between two 125  $\mu\text{m}$  matte-polyester substrates. The active layer contains the active component, a marker dye, stabilizers and other components that give the film its near energy independent response. The thickness of the active layer varies slightly between different production lots. The yellow marker dye incorporated in EBT3, in conjunction with an RGB film scanner and FilmQA software, enables the dosimetry process to benefit from the application of triple-channel dosimetry.

The key technical features of GafChromic EBT3 include:

- Dynamic dose range: 0.1 Gy to 20 Gy;
- Optimum dose range: 0.2 Gy to 10 Gy;
- Real time development without post-exposure treatment;
- Small energy-dependence from 100 keV to MV range;
- Near tissue equivalent;
- High spatial resolution – can resolve features down to 25  $\mu\text{m}$ , or less;
- Proprietary new technology incorporating a marker dye in the active layer;
- Enables non-uniformity correction using multi-channel dosimetry;
- Small decreases UV/visible light sensitivity; and,

- Stable at temperatures up to 60°C.

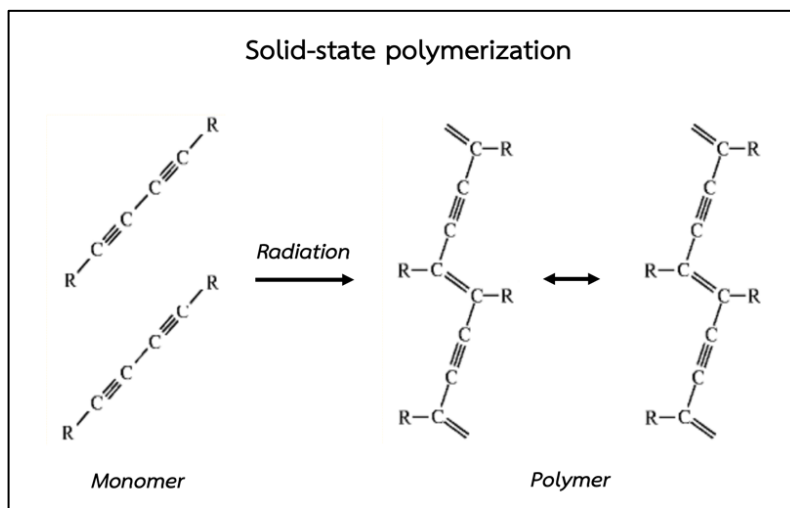


Figure 2. 8 The solid-state polymerization of GafChromic film.

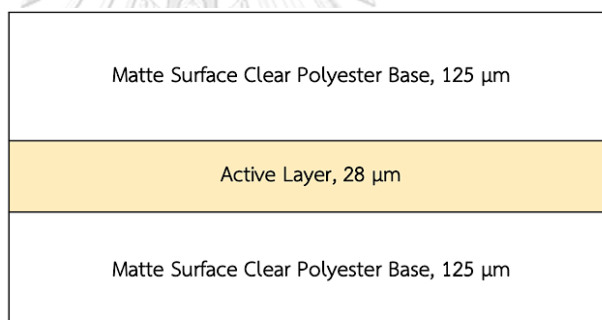


Figure 2. 9 Structure of GafChromic EBT3 dosimetry film.

### 2.1.5.3 Ionization chamber

The ionization chamber (IC) is the simplest of all gas-filled radiation detectors, and the most widely used type for accurate point dose measurement which can be used as an absolute or a relative dosimeter because it consists of numerous strong features. There are independence of energy, dose, dose rate, and direction (depending on the design of IC ex: cylindrical or parallel plate). Besides, the IC also provides dose measurement accuracy, reproducibility, linearity and can be applied with a wide range of clinical photon and electron energies.

For IC operation principle measures the charge from the number of ion pairs (positive and negative charges) created within an inert gas caused by incident radiation. The ion chamber consists of a gas-filled chamber with two electrodes of anode and cathode. A voltage is applied between the electrodes to create an electric field in the fill gas. When gas between the electrodes is ionized by incident ionizing radiation, ion-pairs are created and the resultant positive ions and dissociated electrons move to the opposite polarity electrodes under the influence of the electric field. This generates an ionization current which is measured by an electrometer. All the charges are created by each interaction between the incident radiation and the gas, and it does not involve the gas multiplication mechanisms such as the Geiger-Müller counter or the proportional counter as displayed in figure 2.10. Thus, the chamber cannot discriminate between radiation types (beta or gamma) and cannot produce an energy spectrum of radiation.

The ion chamber has various types and sizes depending on suitable usage, such as cylindrical or thimble, plane-parallel, well-type, extrapolation, and segmented. This study used a cylindrical which has a commercial name of the IBA CC01 ionization chamber.

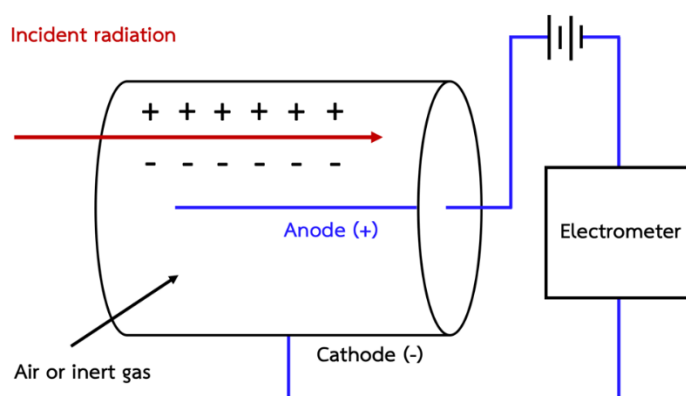


Figure 2. 10 Schematic diagram of the simplest of all gas-filled radiation detector.

### 2.1.6 Plan evaluation

This study used several methods to evaluate the dosimetry results, such as the percent point dose difference and gamma evaluation method.

### 2.1.6.1 The percent point dose difference

For point dosimetry, the percent point dose difference between measured and calculated doses is defined as equation 2.1, while the percent point dose difference between static and dynamic measured doses using equation 2.2. The Quality Assurance (QA) results will pass if the percent dose difference is within criteria such as 3% (28).

$$\% \text{ Point dose difference} = \frac{(\text{Measured dose} - \text{Calculated dose})}{\text{Calculated dose}} \times 100\% \quad (2.1)$$

$$\% \text{ Point dose difference} = \frac{(\text{Dynamic measured dose} - \text{Static measured dose})}{\text{Static measured dose}} \times 100\% \quad (2.2)$$

### 2.1.6.2 Gamma evaluation method

The gamma evaluation method is developed to quantitatively compare 2 or 3 dimensional dose distributions by utilizing the percent dose difference (DD) and distance to agreement (DTA). The DTA is the distance difference between a measured data point and the nearest point in the calculated dose distribution that exhibits the same dose. Regarding the calculation of the DD, there are two types of gamma index methods, which are the global and local gamma index analyses. The global gamma index analysis calculates the DDs relative to the maximum dose (or prescription dose), while the local gamma index analysis calculates the DDs relative to the doses at each evaluated point. The determination of acceptance criteria (29) is considered by an ellipsoid, which is shown in figure 2.11, at the surface. The equation defining the surface is

$$1 = \sqrt{\frac{r^2(r_m, r)}{\Delta d_M^2} + \frac{\delta^2(r_m, r)}{\Delta D_M^2}} \quad (2.3)$$

Where

$$r(r_m, r) = |r - r_m| \quad (2.4)$$

and

$$\delta(r_m, r) = D(r) - D_m(r_m) \quad (2.5)$$

is the dose difference at the position  $r_m$ . If any portion of the  $D_c(r_c)$  surface intersects the ellipsoid defined by equation (2.3), the calculation passes at  $r_m$ . Defining the acceptance criteria not just along the  $\delta$  axis and in the  $r-r_m$  plane allows for a more general comparison between calculation and measurement than does the traditional composite evaluation. The quantity on the right-hand side of equation (2.3) 1 can be used to identify a quality index  $\gamma$  at each point in the evaluation plane  $r-r_m$  for the measurement point  $r_m$ ,

$$\gamma(r_m) = \min\{\Gamma(r-r_m)\} \forall \{r_c\} \quad (2.6)$$

Where

$$\Gamma(r_m, r_c) = \sqrt{\frac{r^2(r_m, r)}{\Delta d_M^2} + \frac{\delta^2(r_m, r)}{\Delta D_M^2}} \quad (2.7)$$

$$r(r_m, r) = |r_c - r_m| \quad (2.8)$$

and

$$\delta(r_m, r_c) = D_c(r_c) - D_m(r_m) \quad (2.9)$$

is the difference between dose values on the calculated and measured distributions, respectively. The pass-fail criteria therefore become

$$\gamma(r_m) \leq 1, \text{ calculation passes,}$$

$$\gamma(r_m) > 1, \text{ calculation fails.}$$

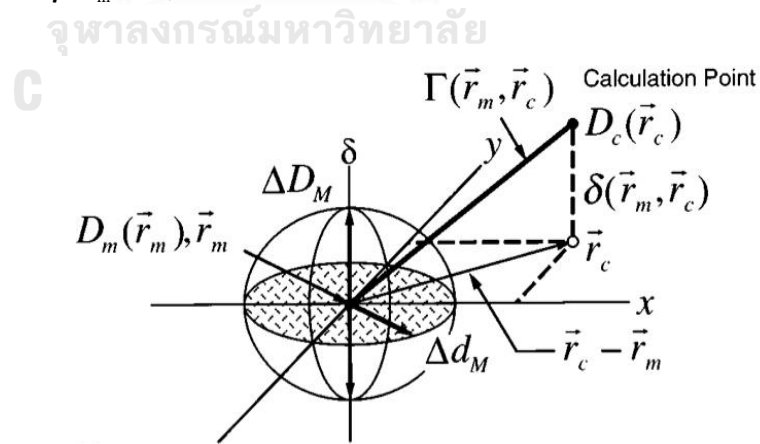


Figure 2. 11 The geometric representation of dose distribution evaluation criteria using the combined ellipsoidal dose-difference and distance-to-agreement tests.

## 2.2 Related works

In the first literature review, Edvardsson A. et al (7) studied motion induced interplay effects of VMAT radiotherapy. This study aimed to use the in-house program to investigate how interplay effects vary with different patients and machine specific parameters. They found that the large interplay effects were observed for individual fractions and the extent varied with the patient and machine specific parameters. Generally, the interplay effects were larger for FFF technique compared to FF technique and increased for higher breathing amplitudes, longer period times, lower dose levels and more complex treatment plans. Also, the interplay effects varied considerably with the initial breathing phase for smaller clinical target volume (CTV) sizes.

In the second literature, the minimizing dose variation from the interplay effect in stereotactic radiation therapy using volumetric modulated arc therapy for lung cancer was performed by Kubo K. et al. (15). This research aimed to investigate the impact of NBs to the dose variation for VMAT-SBRT to lung cancer. They found that the NBs is an important factor to reduce the dose variation caused by the interplay effect with VMAT-SBRT for lung cancer. The patient who breathes > 40 times during irradiation of two partial arcs VMAT may be suitable for VMAT-SBRT for lung cancer. In addition, this paper also showed the interesting parameter that is the interplay effect variable score (IVS). The IVS is defined as equation 2.10.

$$IVS = TMMCS_v \times NBs \quad (2.10)$$

The combination of tumor motion (TMMCS<sub>v</sub>) is defined as equation 2.11.

$$TMMCS_v = MCS_v \div A \quad (2.11)$$

Where

MCS<sub>v</sub> cited from Masi L. et.al study (5) is the combination of the complexity of the MLC sequence and have value range in 0-1.

A is amplitude of tumor in only SI direction.

The results of both values indicated the increasing IVS and TMMCS<sub>v</sub> are associated with lower dose variation.

The third literature review, the report of AAPM task group number 76 (18), illustrated the lung tumor motion data. The results showed that the tumor did not move in only the SI direction as shown in table 2.2, example of the study of Ross CS et al., who found that the greatest direction of

tumor movement was noted in lateral motion (average 9.2 mm in middle lobe and 10.5 mm in lower lobe). The research of Erridge et al. in table 2.2, showed that the lung tumor motion was high in all directions: 12.5 mm for SI, 9.4 mm for AP, and 7.3 mm for LR direction.

Table 2. 2 Lung tumor–motion data. The mean range of motion and the (minimum–maximum).

Observers	Directions (mm)		
	SI	AP	LR
Barnes et al.: Upper, Middle lobe	7.5 (2-11)	-	-
Barnes et al.: Lower lobe	18.5 (9-32)	-	-
Chen et al.	(0-50)		
Ekberg et al.	3.9 (0-12)	2.4 (0-5)	2.3 (0-5)
Engelsman et al.: Upper, Middle lobe	(2-6)	-	-
Engelsman et al.: Lower lobe	(2-9)	-	-
Erridge et al.	12.5 (6-34)	9.4 (5-22)	7.3 (3-12)
Ross et al.: Upper lobe	-	1 (0-5)	1 (0-3)
Ross et al.: Middle lobe	-	0	9 (0-16)
Ross et al.: Lower lobe	-	1 (0-4)	10.5 (0-13)
Grills et al.	(2-30)	(0-10)	(0-6)
Hanley et al.	12 (1-20)	5 (0-13)	1 (0-1)
Murphy et al.	7 (2-15)	-	-
Plathow et al.: Upper lobe	4.3 (2.6-7.1)	2.8 (1.2-5.1)	3.4 (1.3-5.3)
Plathow et al.: Middle lobe	7.2 (4.3-10.2)	4.3 (1.9-7.5)	4.3 (1.5-7.1)
Plathow et al.: Lower lobe	9.5 (4.5-16.4)	6.1 (2.5-9.8)	6.0 (2.9-9.8)
Seppenwoolde et al.	5.8 (0-25)	2.5 (0-8)	1.5 (0-3)
Shimizu et al.	-	6.4 (2-24)	-
Sixel et al.	(0-13)	(0-5)	(0-4)
Stevens et al.	4.5 (0-22)	-	-

AP: anterior-posterior; LR: left-right; SI: superior-inferior.

## CHAPTER 3

### RESEARCH METHODOLOGY

#### 3.1 Research design

This study is an observational analytical study.

#### 3.2 Research design model

The diagram of the research design model is shown in figure 3.1.

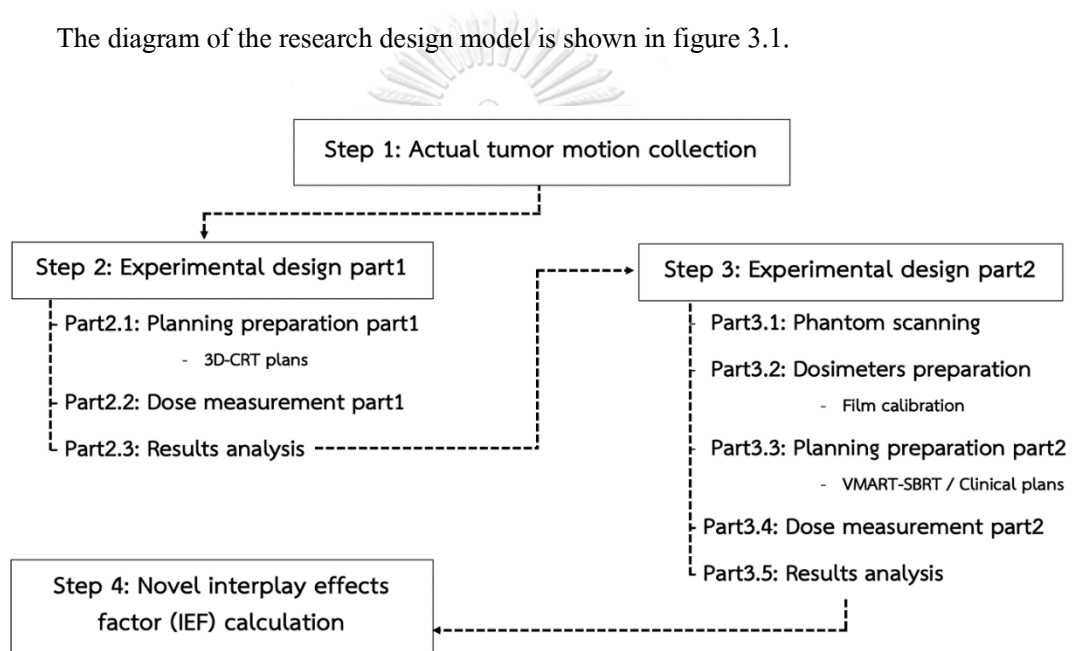


Figure 3. 1 Research design model.

#### 3.3 Conceptual framework

The factors that affect the dosimetric outcomes are the groups of tumor characteristics, breathing pattern, and treatment technique parameters. The diagram of conceptual framework is shown in figure 3.2.



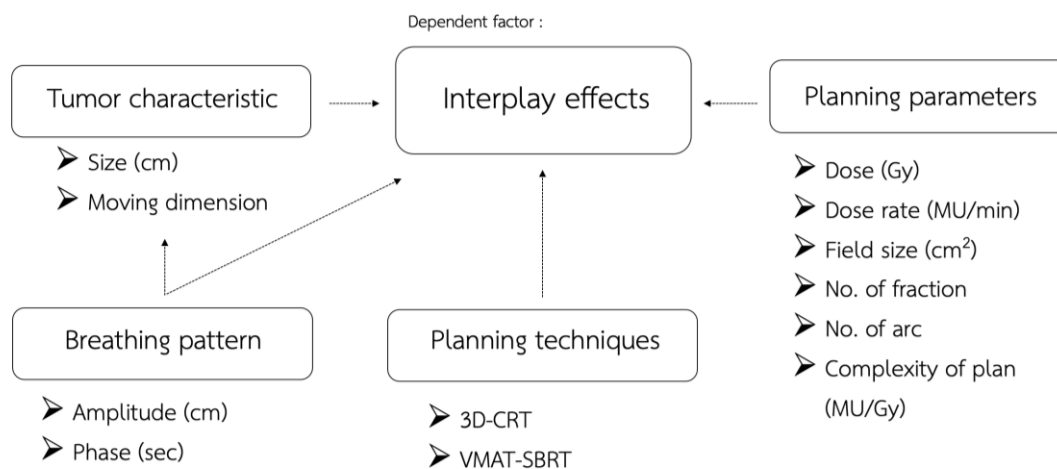


Figure 3. 2 Conceptual frameworks.

### 3.4 Keywords

- Interplay effects
- SBRT
- VMAT
- Lung cancer

### 3.5 Research questions

#### 3.5.1 Primary question: จุฬาลงกรณ์มหาวิทยาลัย

What are the dosimetric parameters that impact of interplay effects in 6 MV FFF photon beams for lung cancer?

#### 3.5.2 Secondary question

What is the novel interplay effect factor (IEF) for VMAT-SBRT lung cancer?

### 3.6 Materials information

The materials used in this study are from the Division of Radiation Oncology, King Chulalongkorn Memorial Hospital. The patient data were collected from the Division of Radiation Oncology, King Chulalongkorn Memorial Hospital during 2019 to 2021.

### 3.6.1 CT simulator (30)

The Philips Brilliance Big Bore CT scanner (Philips Medical Systems, Cleveland, OH, USA) as shown in figure 3.3 is designed as a CT simulator to meet the needs of radiation oncology, focusing on accuracy, patient positioning, imaging performance, and intuitive workflow.

The main features of Big Bore CT are:

- 85 cm bore size to accommodate patients with immobilization;
- 60 cm true Scan Field of View (SFOV) to include all patient skin surface; no compromise when using the scan for radiation dose calculations; and,
- 4DCT tools, to evaluate motion of the tumor and critical organs during breathing to aid in making clinical decisions regarding the size of the target volume and gated treatment delivery. Respiratory correlated gating with third-party gating device connectivity, such as the Real-time Position Management (RPM) System (Varian Medical System, Inc, Palo Alto, CA, USA). It is an accurate, easy-to-use, and provides both respiratory gating for respiration-synchronized imaging and treatment, as well as 3D real-time patient position monitoring. It is comfortable for the patient and accommodates all clinical breathing protocols, including free-breathing (31).



Figure 3. 3 The Philips Brilliance Big Bore CT scanner.

### 3.6.2 Lung patient images

A retrospective group of thirty lung cancer patients who underwent 4DCT with free-breathing conditions and 2-3 full arcs of SBRT-VMAT during 2019-2021 was chosen. The MIP reconstruction images from ten phases of 4DCT images were transferred to Eclipse TPS, where the range of total PTV volumes was 9.1-83.0 cm<sup>3</sup>. The targets are averages located on the middle and upper lobes of both sides of the lung. For organs at risk, the OARs were heart, esophagus, spinal cord, whole lungs (subtract PTV), and contralateral lung.

### 3.6.3 Treatment planning system and dose calculation algorithm

The Eclipse<sup>TM</sup> treatment planning system (TPS) with Anisotropic Analytical Algorithm (AAA) version 15.6 (Varian Medical System, Inc, Palo Alto, CA, USA), which is shown in figure 3.4, was used in this study. This treatment planning is suitable for all treatment techniques such as 3D-CRT, IMRT, and VMAT. The AAA provides a fast and accurate dose calculation for clinical photon beams even in regions of complex tissue heterogeneities.

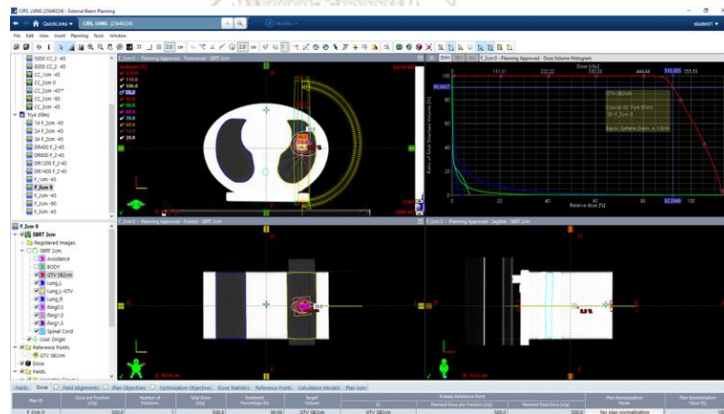


Figure 3. 4 The Eclipse<sup>TM</sup> Treatment Planning System.

### 3.6.4 TrueBeam linear accelerator

The TrueBeam millennium 120 MLC linear accelerator (Varian Medical System, Inc, Palo Alto, CA, USA), is shown in figure 3.5. The machine can be operated in at 6 megavoltage (MV) for photon beams in both flattening filter (FF) and FFF techniques for conventional and stereotactic treatment, respectively. The machine can be provided with a range of field sizes from 0.5 × 0.5

$\text{cm}^2$  to  $40 \times 40 \text{ cm}^2$  at isocenter. The distance from the target to isocenter is 100 cm. The dose rates can be adjusted from 100 to 600 monitor unit per minute (MU/min) for conventional mode, while can be modified from 400 to 2,400 MU/min for stereotactic mode.



Figure 3. 5 The TrueBeam millennium 120 MLC linear accelerator.

### 3.6.5 Phantoms

#### 3.6.5.1 MotionsSimXY/4D dynamic phantom

The MotionSimXY/4D (Sun Nuclear Corporation, Melbourne, FL, USA) in figure 3.6 is intended for the quality assurance (QA) study of motion effects in radiation therapy imaging and delivery by moving a phantom through programmable motion patterns for dosimetric measurement. The platform was designed to be used together with the two-dimensional (2D) diode array using a high precision X-Y motor to drive the MapCHECK2 in X and Y directions (the operating system is the same as the MapCHECK2). Moreover, this platform also allowed a wide range of motor movement, where the maximum travel was 10.2 cm along each X-Y axis and the maximum velocity was 5.08 cm/s.



Figure 3. 6 The MotionsSimXY/4D dynamic phantom with the MapCHECK2.

### 3.6.5.2 Solid water phantom

The virtual water slab phantom (Gammex RMI, Middleton, Wisconsin, USA) is a water-equivalent material which can scatter and attenuate x-rays in the same way as water without charge storage problems. The virtual water slab phantom provides  $1.03 \text{ g/cm}^3$  of the density and 5.97 atomic numbers. This phantom can be used for both photon and electron beams. The phantom's size of  $30 \times 30 \text{ cm}^2$  with various thicknesses as shown in figure 3.6 were used in this study.

### 3.6.5.3 CIRS dynamic thorax phantom model 008A

The CIRS model 008A dynamic thorax phantom (Computerized Imaging Reference System, Inc., Norfolk, VA, USA) in figure 3.7 is a precision instrument for investigating and minimizing the impact of tumor motion inside the lung. It provides known, accurate and repeatable 3D target motion inside a tissue equivalent phantom. The phantom body represents a human thorax, which consists of five structures as listed in table 3.1. The body is connected to a motion actuator box that induces 3D target motion through linear translation and rotation of the lung equivalent rod. Target and surrogate motion are independently controlled with CIRS motion control software. A lung equivalent rod containing spherical targets and various detectors are inserted into the lung equivalent lobe of the phantom. In this study, the microchamber inserts and the SBRT insert were selected to use together with EBT3 films and CC01

dosimeters, respectively. Each rod includes a 1, 2, and 3 cm soft-tissue equivalent target inserted as shown in figures 3.8 and 3.9.

Table 3. 1 Characteristics of the CIRS dynamic thorax phantom components.

Materials	Density (g/cc)	Electron density ( $\times 10^{23}$ , per cc)	Ratio to H <sub>2</sub> O
Plastic Water DT	1.04	3.35	1.00
Lung	0.21	0.69	0.21
Cortical bone	1.91	5.95	1.78
Trabecular bone	1.20	3.86	1.16
Soft tissue target	1.06	3.43	1.03

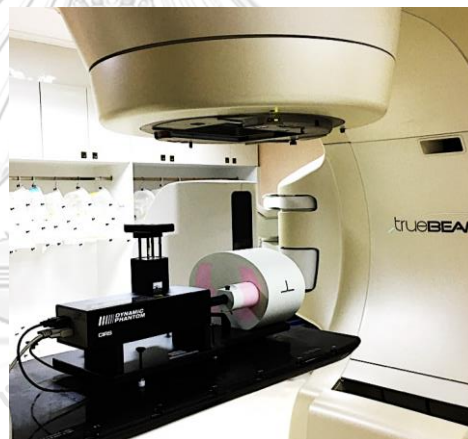


Figure 3. 7 The CIRS model 008A dynamic thorax phantom.

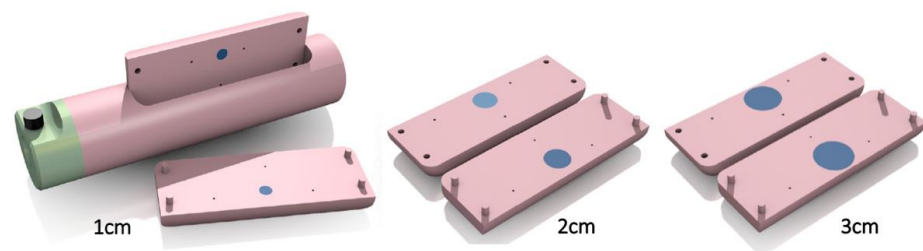


Figure 3. 8 The SBRT insert with 1, 2, and 3 cm diameter of soft-tissue equivalent targets.

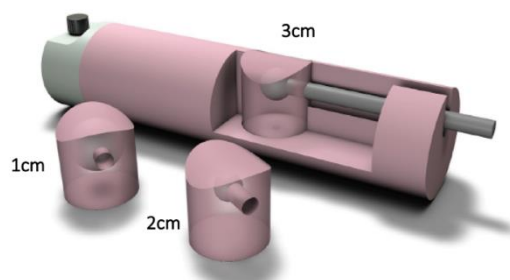


Figure 3. 9 The microchamber insert with 1, 2, and 3 cm diameter of soft-tissue equivalent targets.

### 3.6.6 Detectors

#### 3.6.6.1 MapCHECK2 2D diode array

The MapCHECK2 (Sun Nuclear Corporation, Melbourne, FL, USA) in figure 3.6 is a 2D detector array for accurate and fast verifying planar radiotherapy dose distributions. It offers smaller 1,527 n-type diode detectors placed uniformly throughout the array to provide high sensitivity and proven stability in a large active field size of  $26 \times 32 \text{ cm}^2$ . A real-time electrometer measures every pulse with 50 millisecond (ms) updates. The diode detectors provide pinpoint sized sampling of dose data proven to detect errors over an entire field, both in and out of gradient. Attempts to measure the entire field by increasing the detector size create a blurred measurement in dose gradients. The detector, used together with SNC patient software (Sun Nuclear Corporation, Melbourne, FL, USA) as shown in figure 3.10 This software is able to calculate the gamma passing rate for the entire irradiated volume as well as the gamma passing rate for each corresponding ROI. This study employed this SNC patient software to evaluate the 2D planar dose difference between diode and film measurements.

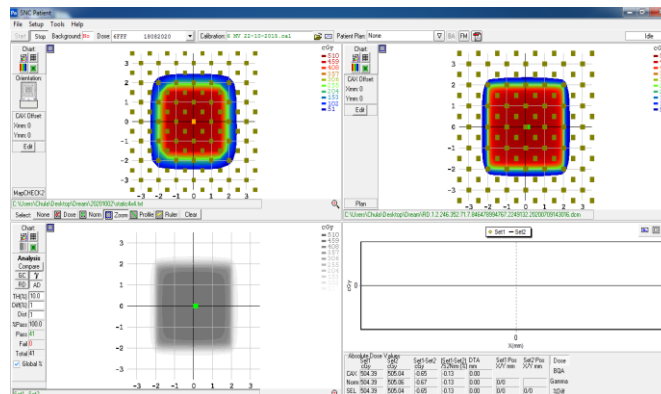


Figure 3. 10 The SNC patient software.

### 3.6.6.2 Gafchromic EBT3 film

The Gafchromic EBT3 self-developing dosimetry film as shown in figure 3.11 (Ashland Inc., Covington, KY, USA) is designed for the measurement of absorbed dose of ionizing radiation. It is particularly suited for high energy photons. The dynamic range of this film is designed for the best performance in the dose range from 0.2 to 10.0 Gy, making it suitable for many applications in IMRT, VMAT and brachytherapy (BT).



Figure 3. 11 The Gafchromic EBT3 self-developing dosimetry film.

### 3.6.6.3 Film scanner

The Epson Perfection V700 Photo (Epson America, Inc., USA), which is shown in figure 3.12, for EBT3 film digitization is used as flatbed scanner. It is a high quality scanner which combines 6400 dots per inch (dpi) maximum hardware



resolution, 48-bit color scanning, and 22 x 30 cm<sup>2</sup> maximum support of media size. The scanner can use together with SNC patient software for plan dose evaluation.

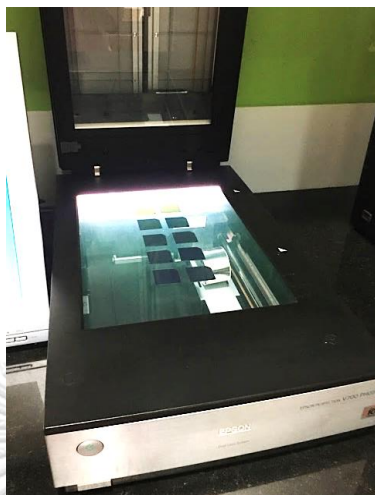


Figure 3. 12 The Epson Perfection V700 Photo film scanner.

#### 3.6.6.4 CC01 ionization chamber

The CC01 (IBA Dosimetry GmbH, Schwarzenbruck, Germany) is a conventional ionization chamber for measurements of small fields and of ranges with high dose gradients, e.g. stereotactic fields as shown in figure 3.13. The active volume, sensitivity, active length, and inner diameter of CC01 are 0.01 cm<sup>3</sup>, 0.0033 nC/cGy, 3.6 mm, 2.0 mm, respectively. This compact chamber is designed for measurements with high reproducibility in air, in solid or in water phantoms. It is suitable for relative dosimetry of photon, electron and proton fields in radiotherapy.



Figure 3. 13 The CC01 ionization chamber.

### 3.6.6.5 Dose1 electrometer

The Dose1 electrometer (IBA Dosimetry, Schwarzenbruck, Germany), which is shown in figure 3.14, is a high precision reference class electrometer for measurements of absorbed dose. It is suitable to use with ionization chambers, semiconductors and diamond probes. For verification of the instrument, connecting cable and proper sensor operation, an electrical check source as well as leakage and bias voltage testing are included as standard built-in features. This electrometer is employed with a 0.01 cm<sup>3</sup> ionization chamber and is set at +300 voltages.



Figure 3. 14 The Dose1 electrometer.

## 3.7 Methods

The method was separated into 4 subparts, namely: 1) Actual tumor motion collection, to collect the longest range of tumor motion in all directions for design the amplitude of phantom motion; 2) Experimental design part1, to investigate the impact of the dosimetric parameters of interplay effects in 6 MV FFF photon beams for lung cancer which was contained the 3D-CRT planning preparation and the dose measurement part1 sections; 3) Experimental design part2, to investigate the impact of the dosimetric parameters of interplay effects in VMAT-SBRT for lung cancer which was contained film calibration, CIRS phantom CT-scanning, VMAT-SBRT planning preparation part2, and dose measurement part2 sections; and, 4) Novel interplay effects factor (IEF) calculation, to calculate the novel IEF for VMAT-SBRT lung cancer.

### 3.7.1 Actual tumor motion collection

#### Materials

1. Lung 4DCT dataset of 9 lung cancer patients who underwent SBRT treatment technique from 2019 to 2020.
2. Eclipse TPS version 15.6 with AAA

#### Methods

1. Select and acquire each lung 4DCT data set in TPS.
2. Adjust the images into the lung window.
3. Play the 4DCT images (10 phases).
4. Notice the maximum motion range in the Y-axis (SI) direction of the tumor (sagittal plane).
5. Measure the longest possible motion distance.
6. Repeat step 2-5 in axial and coronal planes to measure the longest distance in Z-axis (AP) and X-axis (LR) directions, respectively.
7. Obtain the distance range of the actual tumor motion in our hospital to use as a reference moving pattern for the phantom.

### 3.7.2 Experimental design part1

#### 3.7.2.1 Planning preparation part1

##### Material

1. Eclipse TPS version 15.6 with AAA

##### Methods

1. Perform the 3D-CRT planning technique on a solid water phantom CT image using the following planning parameters in table 3.2.
2. Evaluate the plans using a dose volume histogram (DVH).

Table 3. 2 The 3D-CRT planning parameters.

Planning parameters	3D-CRT, 6 MV, 1 AP field, 500 cGy/F, 1400 MU/min, 4x4 cm <sup>2</sup> , 100 cm of SAD, and 5 cm of measurement depth
Planning criteria	Prescribed dose with in at least 95% of the PTV

### 3.7.2.2 Dose measurement part1

#### Materials

1. TrueBeam Varian linear accelerator
2. MotionSimXY/4D dynamic phantom with motion control software
3. MapCHECK2 2D diode array with SNC patient software
4. Solid water phantom

#### Methods

1. Set a dynamic phantom on the couch inside the treatment room.
2. Drive the phantom in 2D orthogonal to the beam's central axis.
3. Place the MapCHECK2 and 3 cm of solid water phantom on the 2D dynamic phantom, respectively as shown in figure 3.15.

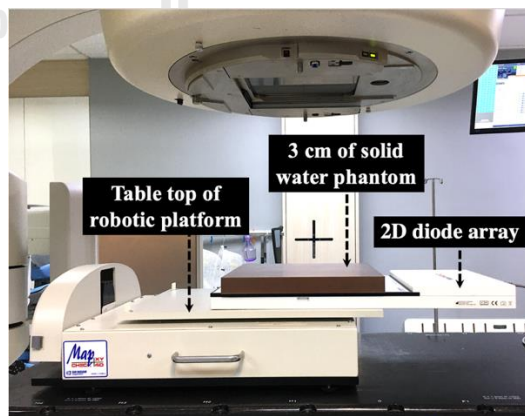


Figure 3. 15 The setting up of the MotionSimXY/4D dynamic phantom, the MapCHECK2, and the solid water phantom.

4. Perform the QA the MapCHECK2 using the SAD technique with a gantry angle of 0 and a field size of 10x10 cm<sup>2</sup>.
5. Measure with 6 MV FFF photon beams and calibrate the dose into 200 cGy.
6. Transfer the 3D-CRT plans to the phantom.
7. Start dose measurements by varying parameters and phantom moving patterns as presented in table 3.3
8. Irradiate the beams for two times in each parameter and compare the dose difference between static and dynamic modes.
9. Record and evaluate the results using the gamma evaluation method in SNC patient software. The criteria used for comparison is the gamma evaluation of 1% dose difference and 1 mm distance to agreement with 10% threshold.

Table 3. 3 All parameters setting of dosimetric measurement part1.

Amplitude	<table border="1"> <thead> <tr> <th>X-axis (cm)</th> <th>Y-axis (cm)</th> </tr> </thead> <tbody> <tr> <td>0</td> <td>0</td> </tr> <tr> <td>- 0.5 to 0.5</td> <td>- 0.5 to 0.5</td> </tr> <tr> <td>- 1 to 1</td> <td>- 1 to 1</td> </tr> <tr> <td>- 2 to 2</td> <td>- 2 to 2</td> </tr> </tbody> </table>	X-axis (cm)	Y-axis (cm)	0	0	- 0.5 to 0.5	- 0.5 to 0.5	- 1 to 1	- 1 to 1	- 2 to 2	- 2 to 2	<table border="1"> <thead> <tr> <th>X-axis (cm)</th> <th>Y-axis (cm)</th> </tr> </thead> <tbody> <tr> <td>- 0.5 to 0.5</td> <td>0</td> </tr> <tr> <td>- 1 to 1</td> <td>0</td> </tr> <tr> <td>- 2 to 2</td> <td>0</td> </tr> </tbody> </table>	X-axis (cm)	Y-axis (cm)	- 0.5 to 0.5	0	- 1 to 1	0	- 2 to 2	0	<table border="1"> <thead> <tr> <th>X-axis (cm)</th> <th>Y-axis (cm)</th> </tr> </thead> <tbody> <tr> <td>0</td> <td>- 0.5 to 0.5</td> </tr> <tr> <td>0</td> <td>- 1 to 1</td> </tr> <tr> <td>0</td> <td>- 2 to 2</td> </tr> </tbody> </table>	X-axis (cm)	Y-axis (cm)	0	- 0.5 to 0.5	0	- 1 to 1	0	- 2 to 2
	X-axis (cm)	Y-axis (cm)																											
	0	0																											
	- 0.5 to 0.5	- 0.5 to 0.5																											
	- 1 to 1	- 1 to 1																											
- 2 to 2	- 2 to 2																												
X-axis (cm)	Y-axis (cm)																												
- 0.5 to 0.5	0																												
- 1 to 1	0																												
- 2 to 2	0																												
X-axis (cm)	Y-axis (cm)																												
0	- 0.5 to 0.5																												
0	- 1 to 1																												
0	- 2 to 2																												
Phase	3, 4, and 5 sec																												
Dose level	5, 8, and 12 Gy																												
Dose rate	400, 600, 800, 1200, and 1400 MU/min																												
Field size	4x4, 6x6, 8x8, and 10x10 cm <sup>2</sup>																												
No. of fraction	1 (10 Gy/1 Fx), 2 (5 Gy/ 2 Fx), and 5 (2 Gy/ 5 Fx)																												

### 3.7.3 Experimental design part2

#### 3.7.3.1 Film calibration

##### Materials

1. TrueBeam Varian linear accelerator
2. Gafchromic EBT3 film
3. Solid water phantom
4. Epson Perfection V700 Photo film scanner

5. SNC patient software

### Methods

1. Prepare 8 pieces of 3x3 cm<sup>2</sup> EBT3 films.
2. Place each film at the center of field size 10x10 cm<sup>2</sup>, at 2 cm depth of 100 cm SAD technique as displayed in figure 3.16.
3. Irradiate the films with 6 MV FFF beams on of various doses (0, 25, 50, 100, 150, 300, 600, 800, and 1000 cGy) for 1,400 MU/min maximum dose rate.
4. Read the optical density of the films using Epson Perfection V700 film scanner with red channel.
5. Plot the calibration curve between dose and optical density.

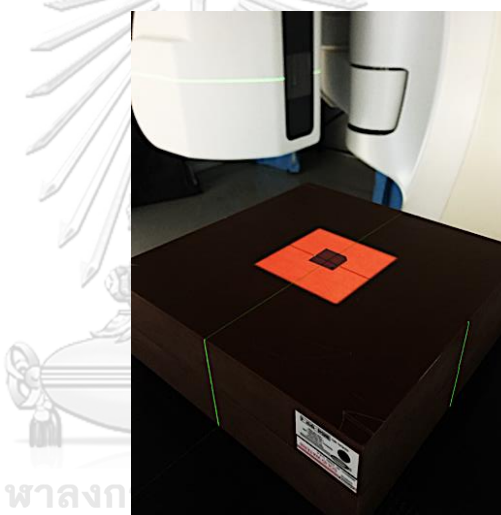


Figure 3. 16 Film calibration setting up on the solid water phantom.

### 3.7.3.2 CIRS phantom CT-scanning

#### Materials

1. Philips Brilliance Big Bore CT scanner
2. CIRS dynamic thorax phantom
3. The 1, 2, and 3 cm diameter of tumor rod and microchamber inserts
4. CC01 ionization chamber

#### Methods

1. Set CIRS phantom with each insert type on the couch inside the CT scanning room. For microchamber rod scanning, we insert the rod together with the CC01 dosimeter. Each insert was scanned at 3 angles at  $0^\circ$ ,  $-45^\circ$ , and  $-90^\circ$  degree position as displayed in figure 3.17.
2. Align the phantom to the external lasers of the CT scanner, then set the phantom to a zero position.
3. Start CT scanning with setting parameters of 120 kVp, 400 mAs, 2 mm of slice thickness on the Big Bore CT scanner.
4. Obtain CIRS CT image datasets for VMAT-SBRT planning.

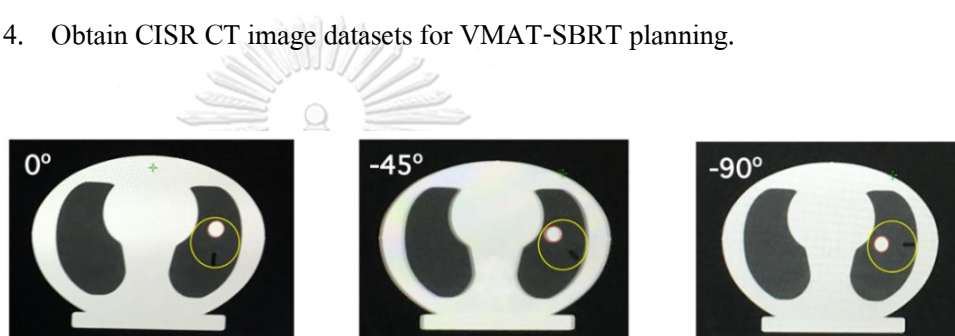


Figure 3. 17 The CT images of CIRS dynamic thorax phantom with CC01 dosimeter and 2 cm diameter of microchamber insert in  $0^\circ$ ,  $-45^\circ$ , and  $-90^\circ$  degrees.

### 3.7.3.3 Planning preparation part2

#### Materials

1. Eclipse TPS version 15.6 with AAA
2. VMAT-SBRT planning of 6 lung patient cases, which each patient provides different information of MU/Gy.

#### Methods

1. Perform VMAT-SBRT planning technique on each CIRS dynamic thorax phantom CT image using following planning parameters in table 3.4
2. Evaluate the plans using dose volume histogram (DVH).
3. Select VMAT-SBRT planning of 6 lung patient cases, which each patient provides different information of MU/Gy, then re-calculate each plan to the CIRS phantom for plan complexity test.

Table 3. 4 The VMAT-SBRT planning parameters.

Planning techniques	VMAT-SBRT, 6 MV, FFF technique, 2 half arcs, 500 cGy/F, 1400 MU/min, 100 cm of SAD, and 0.2 cm of calculation resolution.
Planning criteria	Prescribed dose with in at least 95% of the PTV

### 3.7.3.4 Dose measurement part2

#### Materials

1. The standard VMAT-SBRT plans and the lung VMAT-SBRT clinical plans.
2. TrueBeam Varian linear accelerator
3. CIRS model 008A dynamic thorax phantom with CIRS motion control software
4. Gafchromic EBT3 films
5. Epson Perfection V700 Photo film scanner
6. SNC patient software
7. CC01 ionization chamber
8. Dose1 electrometer

#### Methods

1. Set a CIRS dynamic phantom on the couch inside the treatment room
2. Drive the phantom in 2D orthogonal to the beam's central axis.
3. Connect each insert rod to the dosimeter
4. Transfer the plans to the phantom
5. Start dose measurements by varying various parameters and phantom moving patterns as presented in table 3.5 and 3.6.
6. Expose the beams two times for each parameter to compare the dose difference between static and dynamic modes.
7. Record and evaluate the results using the gamma evaluation method in SNC patient software for film dose measurements, while applying the percent point



dose difference for CC01 dose measurements as mentioned in equation 2.2. The criteria used for comparison is the gamma evaluation of 3% dose difference and 2 mm distance to agreement with 10% threshold following the criteria of AAPM task group number 218 (31) recommendation for SBRT planning technique.

Table 3. 5 All parameters setting of amplitude tests in dose measurement part2.

Parameters		Phantom setting		Planning	Detector type
		Moving pattern	Starting angle of insert (degree)		
Phase	3, 4, 5 sec	3,3,3 mm of XYZ amplitude with vary phases	-45	Standard VMAT-SBRT plans	EBT3 film
Dose rate	4,8,12,14 MU/min	5,10,5 mm of XYZ amplitude with 4 sec of phase			
No. of arc	1,2,3 (Half arc)				
Tumor size	1,2,3 cm of diameter				
Dose	5, 8, 12 Gy				
No. of fraction	1,2,3,4,5 fractions				
Plan complexity	41.50, 60.72, 74.47, 92.67, 97.70, 130.13 MU/Gy of 6 lung patients		Lung VMAT-SBRT clinical plans	CC01 ionization chamber	



Table 3. 6 All parameters setting of phase, dose rate, no. of arc, tumor size, dose, no. of fraction, and plan complexity tests in dose measurement part2.

Parameters				Phantom setting		Planning	Detector type	
Amplitude	Dimension	Axis	Coordinate (mm)	Moving pattern	Starting angle of insert (degree)			
		1D	X	(0,0,0)	Vary amplitudes with 4 sec of phase	0	Standard VMAT-SBRT plans	EBT3 film
(1,0,0)								
(3,0,0)								
(5,0,0)								
Y			(0,1,0)					
			(0,3,0)					
			(0,5,0)					
Z			(0,0,1)	-90				
			(0,0,3)					
		(0,0,5)						
2D		XY	(1,1,0)	Vary amplitudes with 4 sec of phase		0		
			(3,3,0)					
			(5,5,0)					
		XZ	(1,0,1)			-45		
			(3,0,3)					
			(5,0,5)					
		YZ	(0,1,1)			-90		
			(0,3,3)					
			(0,5,5)					
3D		XYZ	(1,1,1)	Vary amplitudes with 4 sec of phase		-90		
	(3,3,3)							
	(5,5,5)							
	(5,10,5)							
	(5,15,5)							
	(5,20,5)							

### 3.7.4 Novel interplay effects factor (IEF) calculation

#### Material

1. All results from both parts of experiments

#### Methods

2. Analyze only parameters that affect the interplay effects for VMAT-SBRT lung cancer. then, create an equation based on the results.

3. Define the scale of score for each parameters according to the results.
4. Select 29 clinical retrospective cases who underwent lung SBRT treatment for test the IEF equation.
5. Find out an ideal and the best cut point of IEF to be used as a need of respiratory motion management suggestion.

### **3.8 Outcome measurement**

#### **3.8.1 Part of dose measurements**

The percent of gamma passing rate and point dose differences

#### **3.8.2 Part of novel interplay effects factor calculation**

Interplay effects factor (IEF)

### **3.9 Expected benefits**

#### **3.9.1 Primary benefit**

Obtain the dosimetric parameters which affect the interplay effects especially 3D-CRT and VMAT-SBRT lung cancer.

#### **3.9.2 Secondary benefit**

Obtain a new dosimetric parameter which can indicate the interplay effects especially in VMAT-SBRT lung cancer patients. The novel dosimetric parameter is used as the treatment plan suggestion and the need of respiratory motion management recommendation.

#### **3.10 Ethical consideration**

Although this study was performed in a phantom, however, the ethical approval was processed by the Ethics Committee of the Faculty of Medicine, Chulalongkorn University (IRB No. 470/63). The certificate is shown in figure 3.18



COA No. 905/2020  
IRB No. 470/63

**คณะกรรมการพิจารณาจริยธรรมการวิจัย  
คณะแพทยศาสตร์ จุฬาลงกรณ์มหาวิทยาลัย**  
1873 ถ.พระราม 4 เขตปทุมวัน กรุงเทพฯ 10330 โทร. 0-2256-4493

---

**เอกสารรับรองโครงการวิจัย**

คณะกรรมการจริยธรรมการวิจัยในคน คณะแพทยศาสตร์ จุฬาลงกรณ์มหาวิทยาลัย ดำเนินการให้การรับรองโครงการวิจัยตามแนวทางหลักจริยธรรมการวิจัยในคนที่เป็นมาตรฐานสากลได้แก่ Declaration of Helsinki, The Belmont Report, CIOMS Guideline และ International Conference on Harmonization in Good Clinical Practice หรือ ICH-GCP

**ชื่อโครงการ** : ผลทางรังสีต่อสถานะอินเตอร์เพลย์สำหรับผู้ป่วยมะเร็งปอดที่ได้รับการรักษาด้วยเทคนิครังสีร่วมพิกัดบริเวณลำตัว

**เลขที่โครงการวิจัย** : -

**ผู้วิจัยหลัก** : นางสาววรรณิศา พูลนาผล

**สังกัดหน่วยงาน** : ภาควิชารังสีวิทยา คณะแพทยศาสตร์ จุฬาลงกรณ์มหาวิทยาลัย

**วิธีทบทวน** : แบบเร่งด่วน

**รายงานความก้าวหน้า** : ส่งรายงานความก้าวหน้าอย่างน้อย 1 ครั้ง/ปี หรือส่งรายงานฉบับสมบูรณ์หากดำเนินการโครงการเสร็จสิ้นก่อน 1 ปี

**เอกสารรับรอง** :

1. โครงร่างการวิจัย Version 2 Date 02/07/2020
2. โครงการวิจัยฉบับย่อ Version 1 Date 27/05/2020
3. Case record form Version 1 Date 27/05/2020
4. Curriculum Vitae and GCP Training
  - Miss Vanida Poolnapol
  - Dr. Taweap Sanghangthum
  - Dr. Mintra Keawsamur

ลงนาม 

(รองศาสตราจารย์นายแพทย์อรเทพ ใจสำราญ)  
รองประธานปฏิบัติหน้าที่แทนประธาน  
คณะกรรมการพิจารณาจริยธรรมการวิจัย

ลงนาม 

(ผู้ช่วยศาสตราจารย์ ดร.พญ.ประภาพรณ รัชตะปิติ)  
กรรมการและเลขานุการ  
คณะกรรมการพิจารณาจริยธรรมการวิจัย

**วันที่รับรอง** : 16 กรกฎาคม 2563  
**วันหมดอายุ** : 15 กรกฎาคม 2564

ทั้งนี้ การรับรองนี้มีเงื่อนไขดังที่ระบุไว้ด้านหลังทุกข้อ (ดูด้านหลังของเอกสารรับรองโครงการวิจัย)

Figure 3. 18 The certificate of approval from ethic committee of the Faculty of Medicine Chulalongkorn University.

## CHAPTER 4

### RESULTS

#### 4.1 Actual tumor motion collection

The longest distances of actual tumor motion in each direction of 9 lung cancer patients who underwent SBRT treatment technique from 2019 to 2020 are presented in table 4.1. The results showed that the tumor moved in all directions with the significant highest of tumor movement in SI direction. The average movement in each direction was  $0.22 \pm 0.16$  cm,  $0.81 \pm 0.56$  cm, and  $0.19 \pm 0.25$  cm of the X-axis, Y-axis, and Z-axis, respectively.

Table 4. 1 The longest distance of actual tumor motion in each direction of 9 lung cancer patients who underwent SBRT treatment technique.

Pt. No.	Tumor No.	Longest tumor distance measurement (cm)		
		X	Y	Z
1	1	0.02	0.65	0.00
2	2	0.27	0.19	0.48
3	3	0.16	1.35	0.00
	4	0.14	0.16	0.14
4	5	0.01	1.65	0.00
5	6	0.26	1.49	0.00
6	7	0.42	1.23	0.00
	8	0.34	0.38	0.23
7	9	0.09	0.39	0.14
8	10	0.22	0.3	0.36
9	11	0.54	1.10	0.76
Average		0.22	0.81	0.19
Standard deviation		0.16	0.56	0.25

## 4.2 Experiment part1

### 4.2.1 Amplitude test

The gamma passing rates of 1%, 1mm criteria of 3D-CRT plans irradiation with different amplitudes and unpaired t-test statistical analysis between 1D (X or Y-axis) and 2D (XY-axis) moving patterns are shown in table 4.2. The results showed the linear decreasing tendency between the gamma passing rates and amplitudes. The higher amplitudes received lower gamma passing rates in all moving patterns, especially for 2D motion (XY-axis). Nevertheless, these comparisons did not show statistically significant differences in the results between 1D and 2D motion since all p-values received exceeded 0.05. The correlation between gamma passing rates and amplitudes was explained by a mathematical linear equation in the form of negative direct variation, as shown in figure 4.1, 4.2, and 4.3. The  $R^2$  of the three curves were higher than 0.90, which can confirm the good negative agreement between gamma passing rate and motion in different amplitudes.

Table 4. 2 The gamma passing rates of 1%, 1mm criteria of 3D-CRT plans irradiation with different amplitudes and unpaired t-test statistical analysis between 1D (X or Y-axis) and 2D (XY-axis) moving patterns.

Amplitude (mm)	Gamma passing rate of 1%, 1mm (%)			Unpaired t-test (p-value)	
	X-axis	Y-axis	Z-axis	X vs XY	Y vs XY
0	100.00	100.00	100.00	-	-
± 5	86.10	88.80	72.40	0.72	0.93
± 10	55.80	60.50	35.20	0.31	0.25
± 20	19.20	24.50	12.30	0.27	0.10

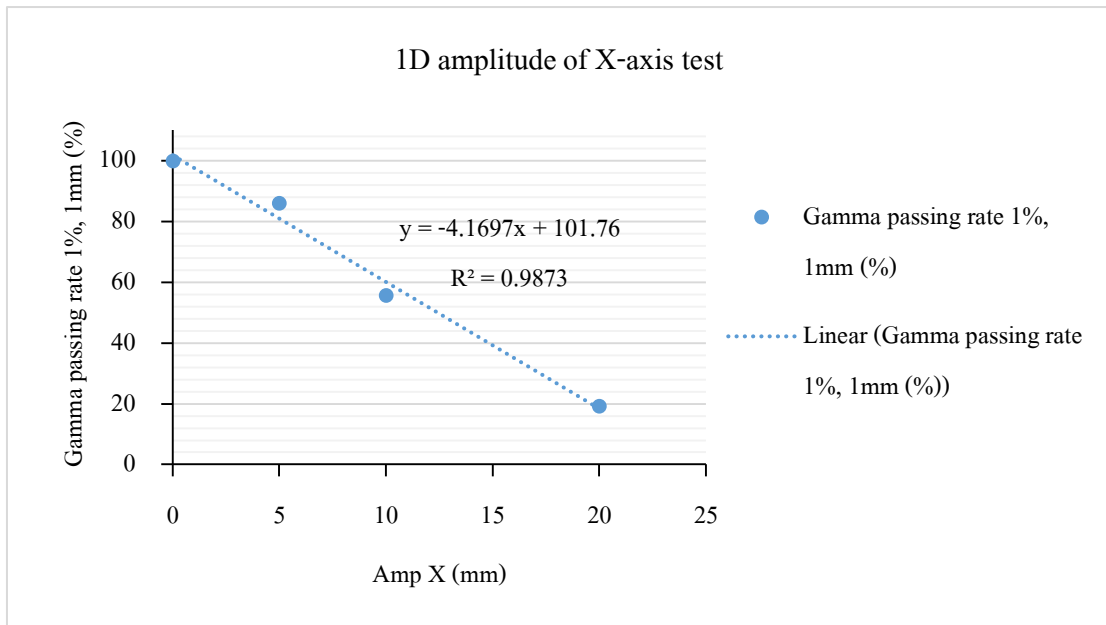


Figure 4. 1 The correlation curves of 1D moving patterns between the gamma passing rates and the different X amplitudes.

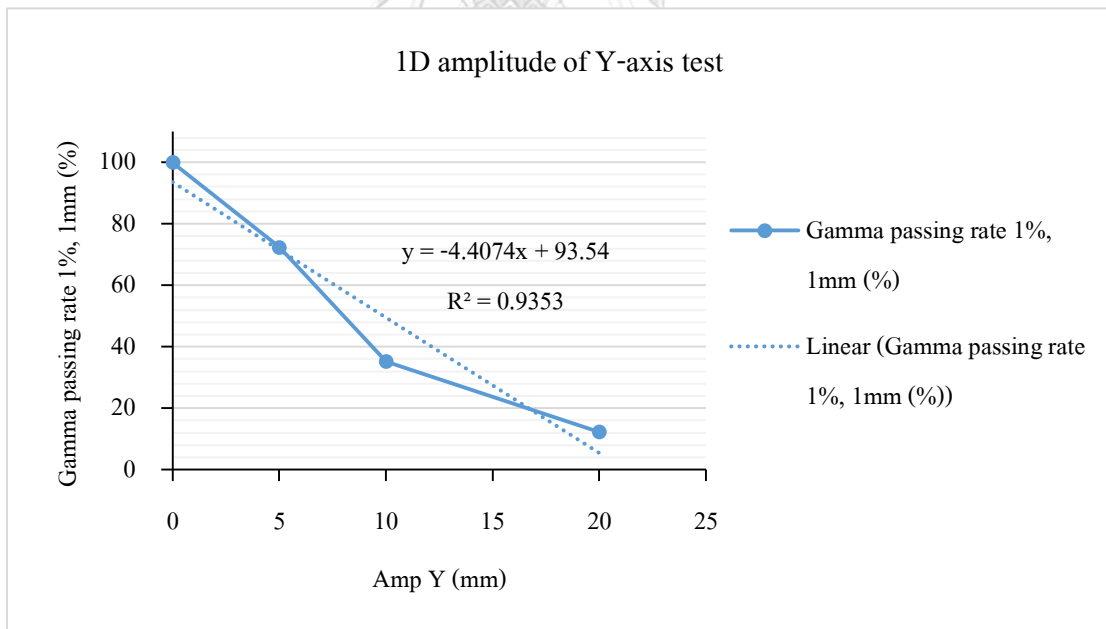


Figure 4. 2 The correlation curves of 1D moving patterns between the gamma passing rates and the different Y amplitudes.

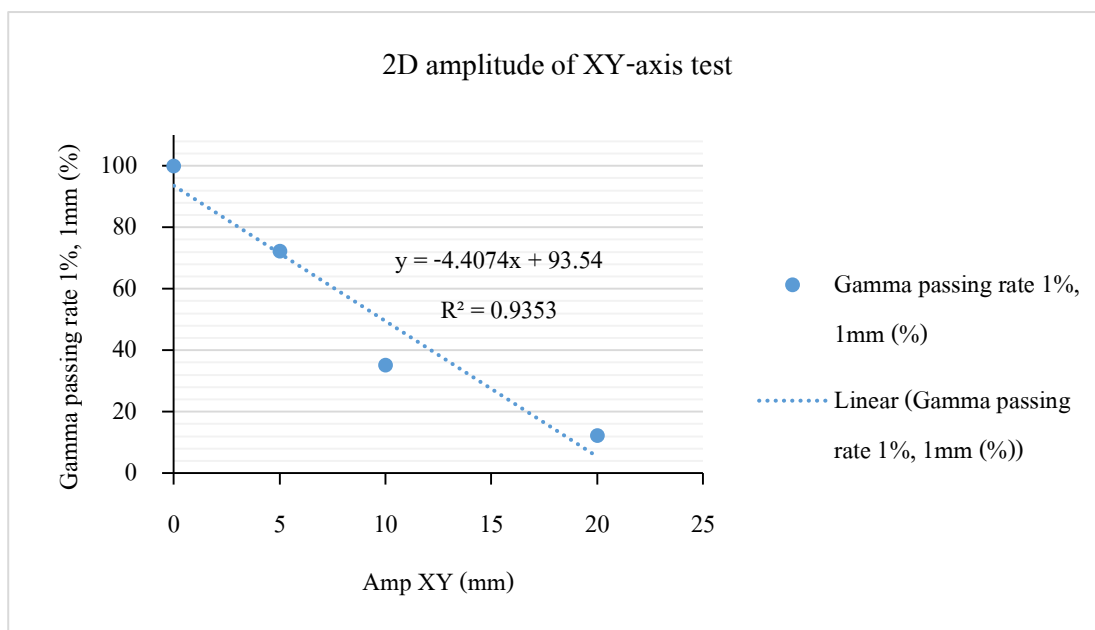


Figure 4. 3 The correlation curves of 2D moving patterns between the gamma passing rates and the different XY amplitudes.

#### 4.2.2 Phase test

The gamma passing rates of 1%, 1mm criteria of 3D-CRT plans irradiation with different phases revealed a constant trend of the results as shown in table 4.3.

Table 4. 3 The gamma passing rates of 1%, 1mm criteria of 3D-CRT plans irradiation with different phases.

Phase (sec)	Gamma passing rate of 1%, 1mm (%)
3	53.10
4	53.10
5	53.10
Average	53.10
Standard deviation	0.00



### 4.2.3 Field sizes test

The gamma passing rates of 1%, 1mm criteria of 3D-CRT plans irradiation with different field sizes are shown in table 4.4. Figure 4.4 exhibited an increasing tendency of gamma passing rates with different symmetric field sizes. The correlation curve illustrates the positive direct variation of the mathematical linear equation together with approximately  $R^2$  of 0.92.

Table 4. 4 The gamma passing rates of 1%, 1mm criteria of 3D-CRT plans irradiation with different field sizes.

Field size (cm <sup>2</sup> )	Gamma passing rate of 1%, 1mm (%)
4	55.00
6	70.00
8	77.00
10	81.00
Average	70.80
Standard deviation	11.44

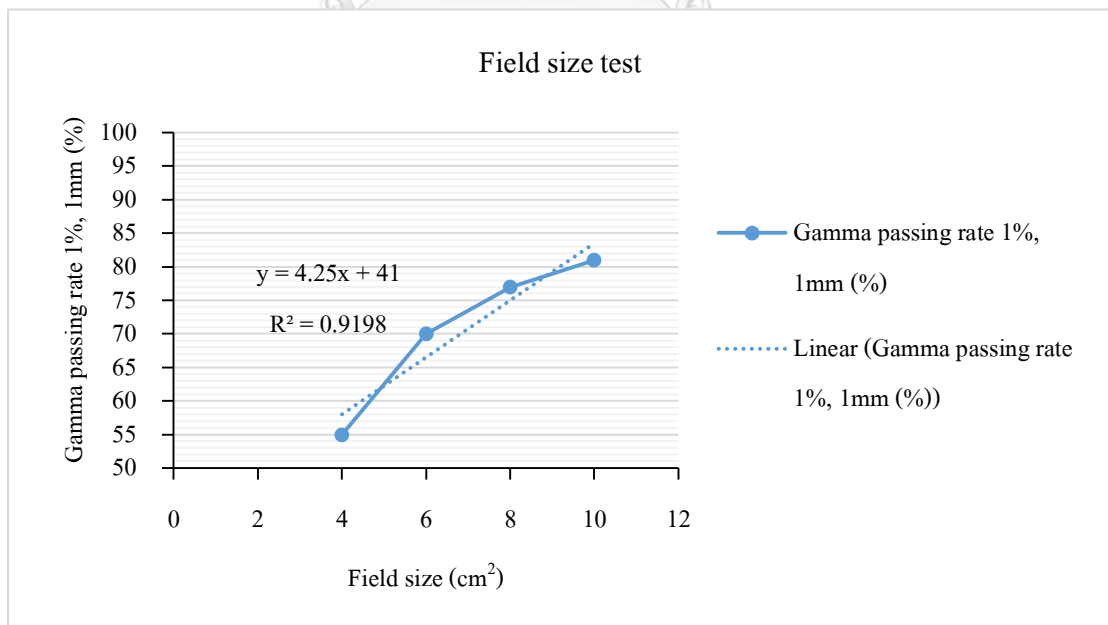


Figure 4. 4 The correlation curves of 2D moving patterns between the gamma passing rates and the different field sizes.

#### 4.2.4 Dose test

The gamma passing rates of 1%, 1mm criteria of 3D-CRT plans irradiation with different doses revealed a constant trend of the results as shown in table 4.5.

Table 4. 5 The gamma passing rates of 1%, 1mm criteria of 3D-CRT plans irradiation with different doses.

Dose (Gy)	Gamma passing rate of 1%, 1mm (%)
5	55.10
8	55.10
12	55.10
Average	55.10
Standard deviation	0.00

#### 4.2.5 Dose rate test

The gamma passing rates of 1%, 1mm criteria of 3D-CRT plans irradiation with different dose rates revealed a constant trend of the results as shown in table 4.6.

Table 4. 6 The gamma passing rates of 1%, 1mm criteria of 3D-CRT plans irradiation with different dose rates.

Dose rate (MU/min)	Gamma passing rate of 1%, 1mm (%)
4	36.70
6	34.70
8	34.70
10	36.70
12	34.70
14	34.70
Average	35.40
Standard deviation	1.00

#### 4.2.6 No. of fraction test

The gamma passing rates of 1%, 1mm criteria of 3D-CRT plans irradiation with different no. of fractions revealed a constant trend of the results as shown in table 4.7.

Table 4. 7 The gamma passing rates of 1%, 1mm criteria of 3D-CRT plans irradiation with different no. of fractions.

No. of fraction	Gamma passing rate of 1%, 1mm (%)
1	36.70
2	34.70
5	36.70
Average	36.00
Standard deviation	1.20

### 4.3 Experiment part2

#### 4.3.1 Film calibration

The relation between absorbed dose and pixel value (scanner response) was plotted and displayed in figure 4.5. The exponential curve was observed. The pixel value decreased when the absorbed dose increased. The high gradient was illustrated in low dose region from 0 to 300 cGy and in the low gradient started from 300 to 1,000 cGy.

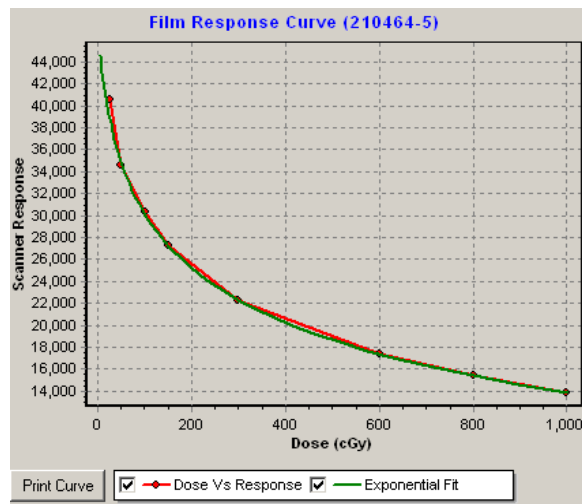


Figure 4. 5 The film calibration curve between absorbed dose and pixel value.

#### 4.3.2 1D amplitude tests

The gamma passing rates of 3%, 2mm criteria of VMAT-SBRT plan irradiation with different 1D amplitudes of X-axis, Y-axis, and Z-axis were shown in tables 4.8, 4.9, and 4.10, respectively. The results showed that there is a decreasing tendency between the gamma passing rates and amplitudes. The higher amplitudes showed lower gamma passing rates in all moving directions. In addition, the correlation between gamma passing rates and amplitudes were explained by a mathematical linear equation in the form of negative direct variation as shown in figure 4.6, 4.7, and 4.8. The  $R^2$  of these three curves were higher than 0.85.

Table 4. 8 The gamma passing rates of 3%, 2mm criteria of VMAT-SBRT irradiation with different 1D amplitudes of X-axis.

Amp X (mm)	Gamma passing rate of 3%, 2mm (%)
	(Static vs Dynamic mode)
± (0,0,0)	100.00
± (1,0,0)	99.80
± (3,0,0)	96.50
± (5,0,0)	93.30
Average	97.40
Standard deviation	3.17

Table 4. 9 The gamma passing rates of 3%, 2mm criteria of VMAT-SBRT irradiation with different 1D amplitudes of Y-axis.

Amp Y (mm)	Gamma passing rate of 3%, 2mm (%) (Static vs Dynamic mode)
$\pm (0,0,0)$	100.00
$\pm (0,1,0)$	100.00
$\pm (0,3,0)$	95.20
$\pm (0,5,0)$	81.00
Average	94.05
Standard deviation	8.99

Table 4. 10 The gamma passing rates of 3%, 2mm criteria of VMAT-SBRT irradiation with different 1D amplitudes of Z-axis.

Amp Z (mm)	Gamma passing rate of 3%, 2mm (%) (Static vs Dynamic mode)
$\pm (0,0,0)$	100.00
$\pm (0,0,1)$	99.70
$\pm (0,0,3)$	89.40
$\pm (0,0,5)$	80.70
Average	92.45
Standard deviation	9.25

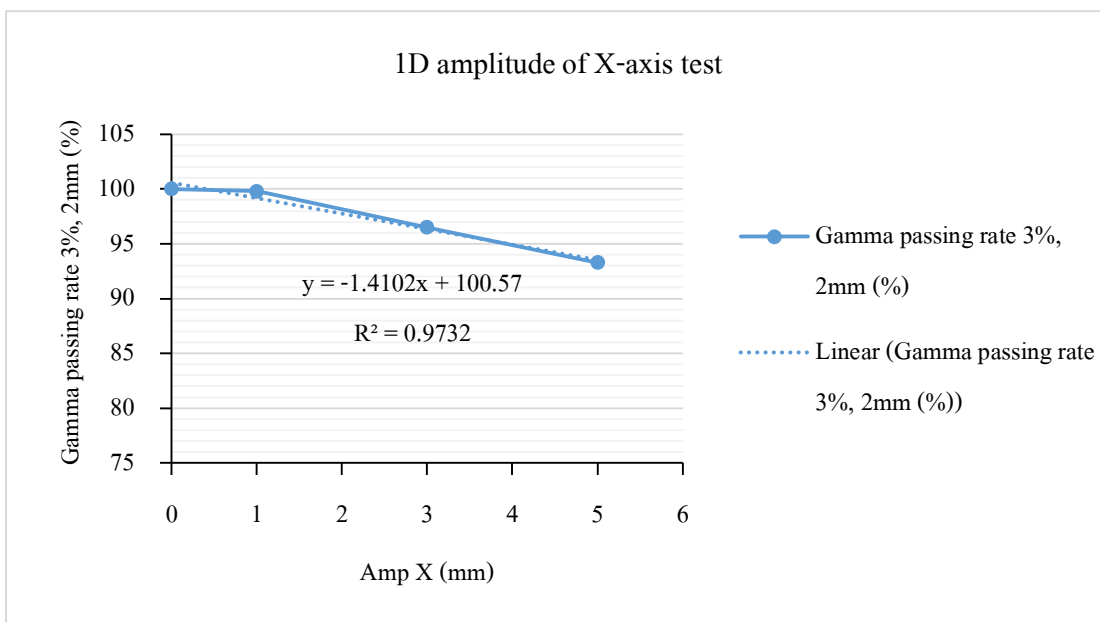


Figure 4. 6 The correlation curves of 1D moving patterns between the gamma passing rates and the different X amplitudes.

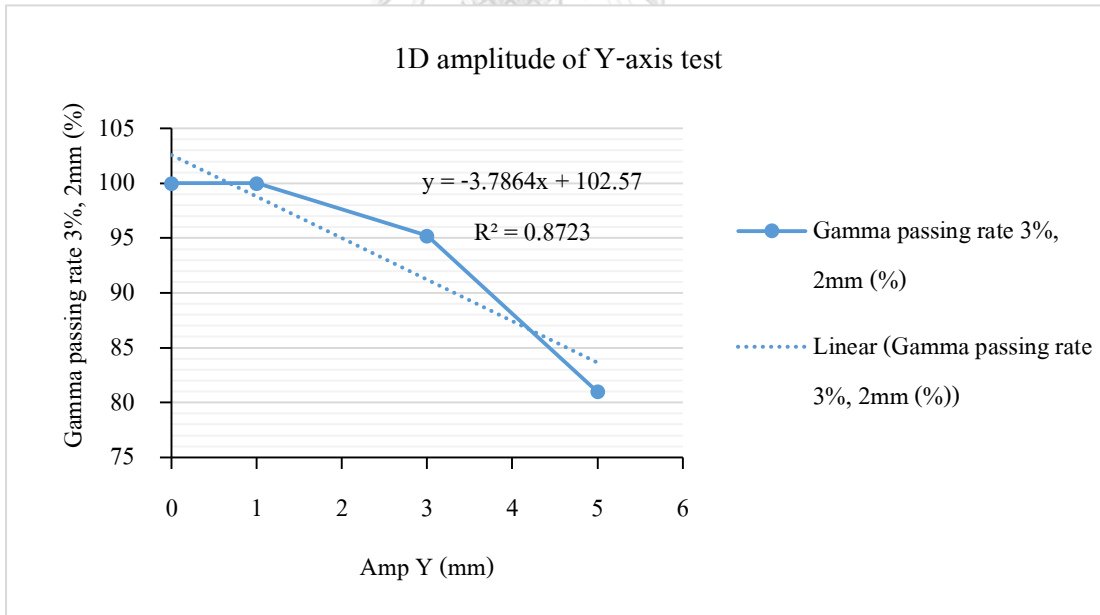


Figure 4. 7 The correlation curves of 1D moving patterns between the gamma passing rates and the different Y amplitudes.

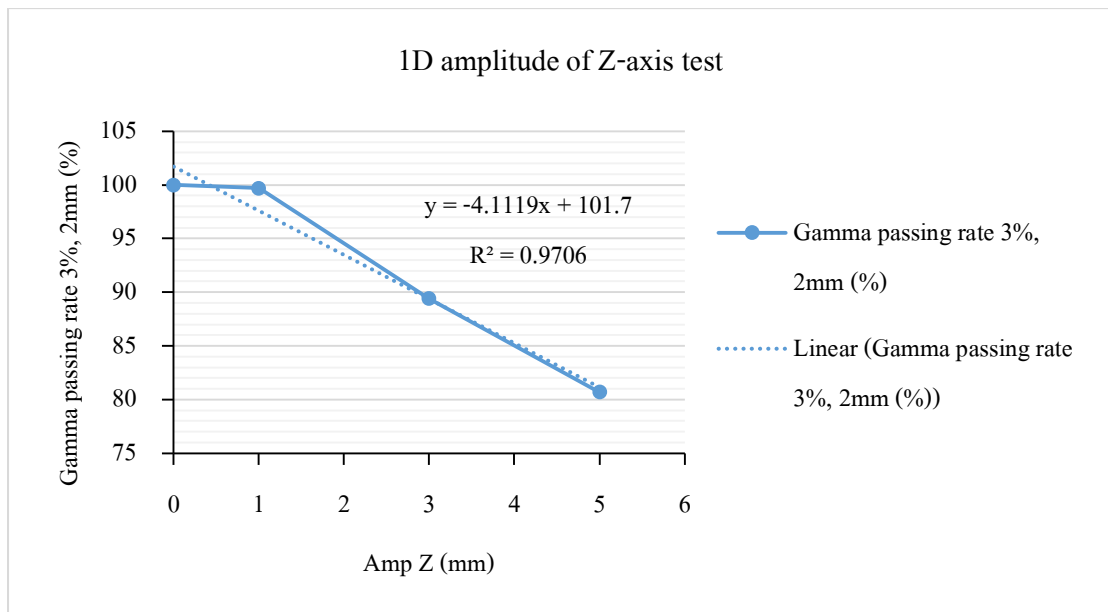


Figure 4. 8 The correlation curves of 1D moving patterns between the gamma passing rates and the different Z amplitudes.

#### 4.3.3 2D amplitude tests

Tables 4.11, 4.12, and 4.13 show the gamma passing rates of 3%, 2mm criteria of VMAT-SBRT plan irradiation with different amplitudes of the XY-axis, XZ-axis, and YZ-axis, respectively. The results also showed a decreasing tendency between the gamma passing rates and amplitudes. The higher amplitudes received lower gamma passing rates in all moving directions. The correlation between gamma passing rates and amplitudes were explained by a mathematical linear equation in the form of negative direct variation, as shown in figures 4.9, 4.10, and 4.11. The  $R^2$  of the three curves provided more than 0.80.

Table 4. 11 The gamma passing rates of 3%, 2mm criteria of VMAT-SBRT irradiation with different 2D amplitudes of XY-axis.

Amp XY (mm)	Gamma passing rate of 3%, 2mm (%) (Static vs Dynamic mode)
$\pm (0,0,0)$	100.00
$\pm (1,1,0)$	96.20
$\pm (3,3,0)$	96.00
$\pm (5,5,0)$	83.80
Average	94.00
Standard deviation	7.04

Table 4. 12 The gamma passing rates of 3%, 2mm criteria of VMAT-SBRT irradiation with different 2D amplitudes of XZ-axis.

Amp XZ (mm)	Gamma passing rate of 3%, 2mm (%) (Static vs Dynamic mode)
$\pm (0,0,0)$	100.00
$\pm (1,0,1)$	99.90
$\pm (3,0,3)$	96.90
$\pm (5,0,5)$	83.30
Average	95.03
Standard deviation	7.95



Table 4. 13 The gamma passing rates of 3%, 2mm criteria of VMAT-SBRT irradiation with different 2D amplitudes of YZ-axis.

Amp YZ (mm)	Gamma passing rate at 3%, 2mm (%) (Static vs Dynamic mode)
$\pm (0,0,0)$	100.00
$\pm (0,1,1)$	98.90
$\pm (0,3,3)$	83.70
$\pm (0,5,5)$	81.60
Average	91.05
Standard deviation	9.75

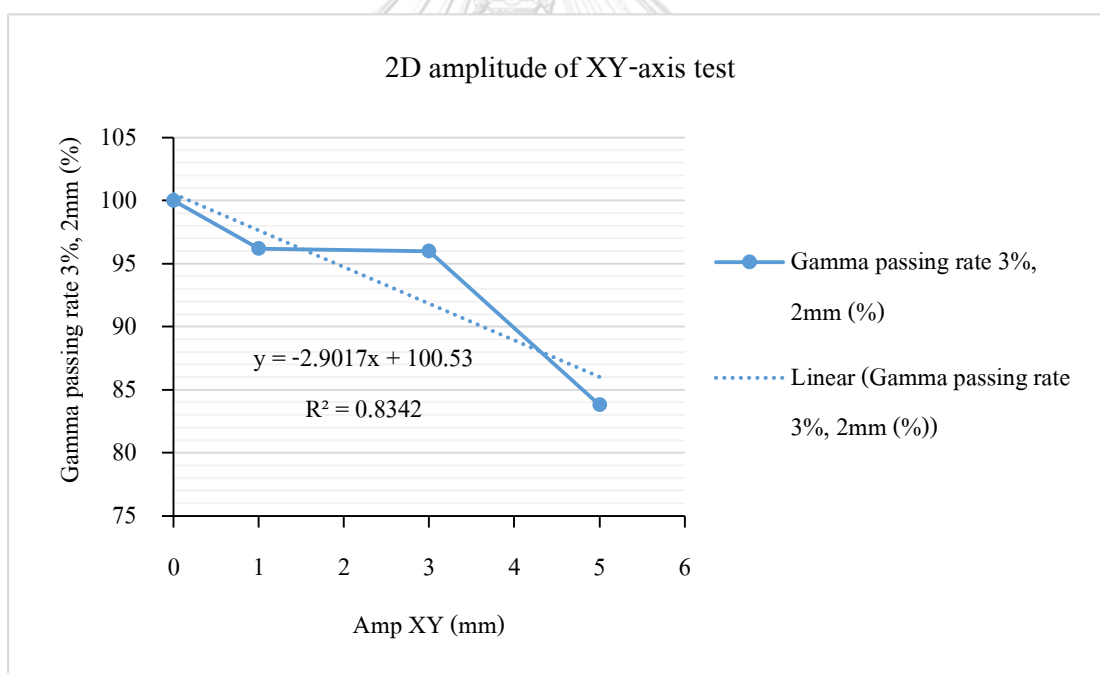


Figure 4. 9 The correlation curves of 2D moving patterns between the gamma passing rates and the different XY amplitudes.

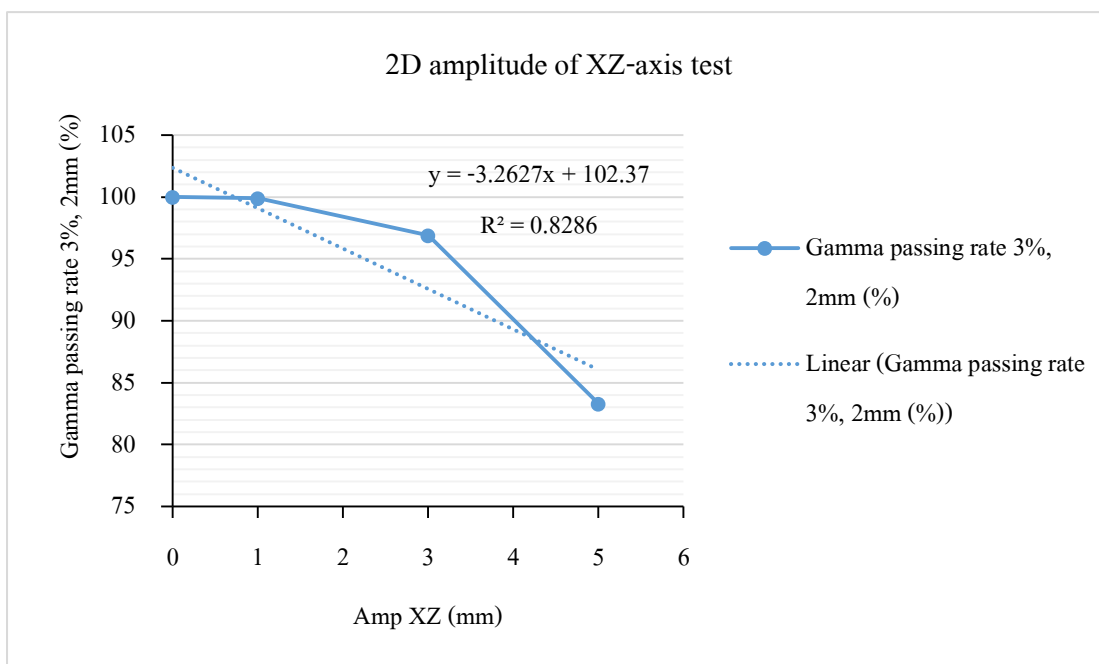


Figure 4. 10 The correlation curves of 2D moving patterns between the gamma passing rates and the different XZ amplitudes.

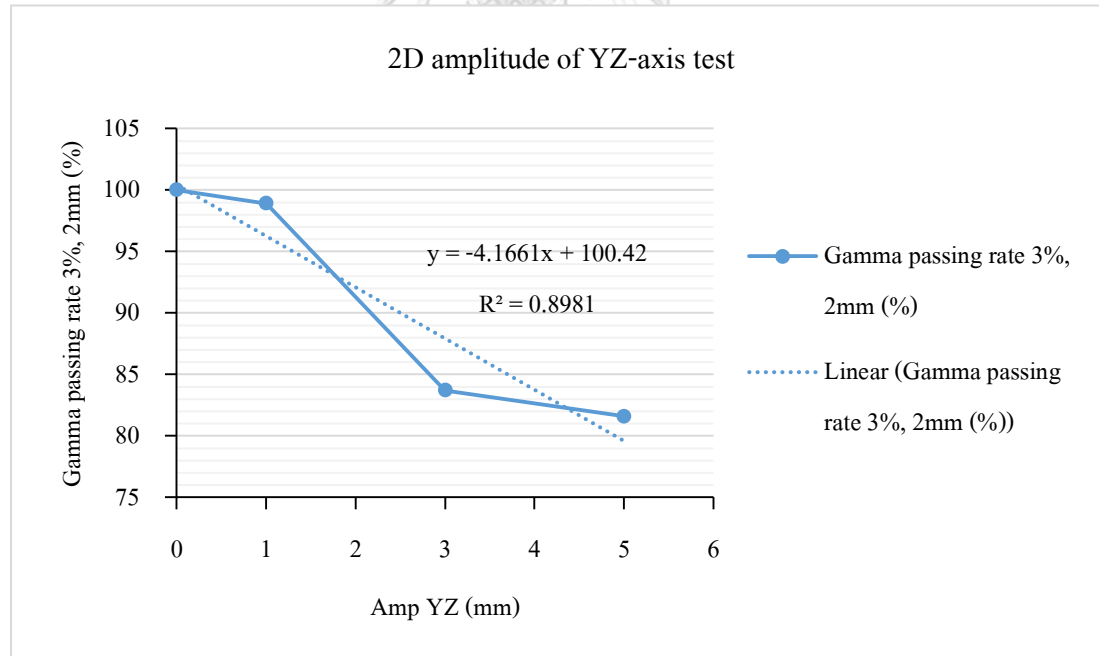


Figure 4. 11 The correlation curves of 2D moving patterns between the gamma passing rates and the different YZ amplitudes.

#### 4.3.4 3D amplitude tests

The gamma passing rates of 3%, 2mm criteria of VMAT-SBRT plan irradiation with different 3D amplitudes of the XYZ-axis, were illustrated in table 4.14. The outcomes were similar to the 1D and 2D as well, which showed a decreasing tendency between the gamma passing rates and amplitudes. The higher amplitudes received lower gamma passing rates. The correlation between gamma passing rates and amplitudes was explained by a mathematical linear equation in the form of negative direct variation, as shown in figure 4.12. The  $R^2$  of the three curves provided more than 0.90.

Table 4. 14 The gamma passing rates of 3%, 2mm criteria of VMAT-SBRT irradiation with different 3D amplitudes of XYZ-axis.

Amp XYZ (mm)	Gamma passing rate of 3%, 2mm (%) (Static vs Dynamic mode)
$\pm (0,0,0)$	100.00
$\pm (1,1,1)$	99.90
$\pm (3,3,3)$	83.90
$\pm (5,5,5)$	79.70
$\pm (5,10,5)$	49.70
$\pm (5,15,5)$	17.80
$\pm (5,20,5)$	17.80
Average	64.11
Standard deviation	35.83

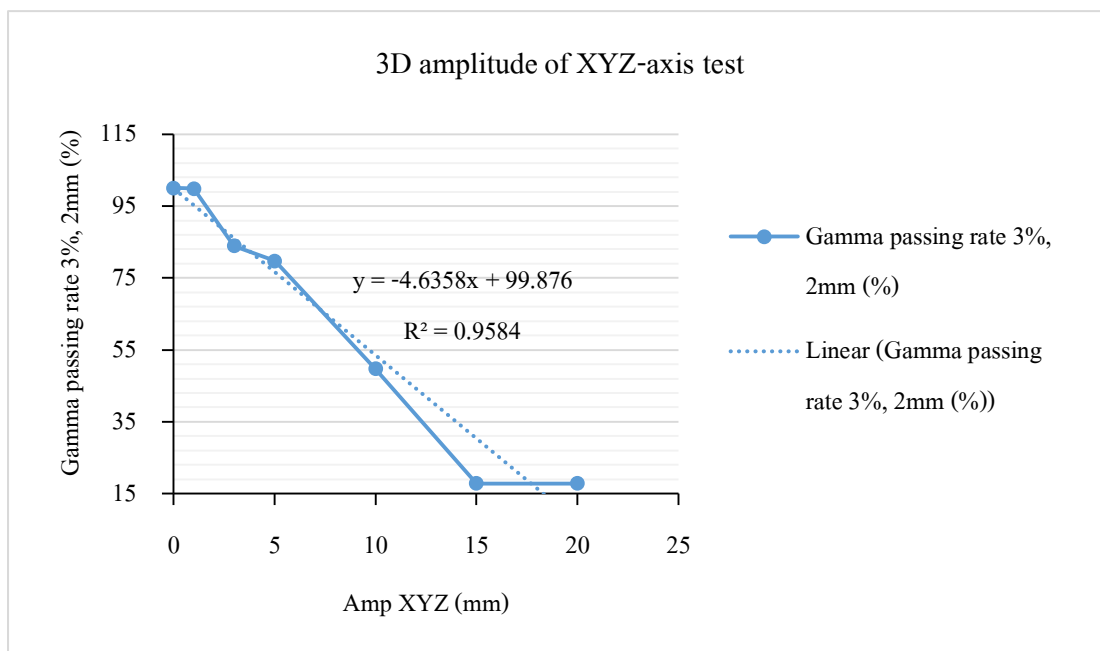


Figure 4. 12 The correlation curves of 3D moving patterns between the gamma passing rates and the different XYZ amplitudes.

#### 4.3.5 Phase test

The gamma passing rates of 3%, 2mm criteria of VMAT-SBRT plans irradiation with different phases revealed a constant trend of the results as shown in table 4.15.

Table 4. 15 The gamma passing rates of 3%, 2mm criteria of VMAT-SBRT plans irradiation with different phases.

Phase (sec)	Gamma passing rate of 3%, 2mm (%)
	(Static vs Dynamic mode)
3	80.20
4	78.20
5	79.20
Average	79.20
Standard deviation	1.00

#### 4.3.6 Tumor size test

The gamma passing rates of 3%, 2mm criteria of VMAT-SBRT plans irradiation with different of tumor sizes revealed a constant trend of the results as shown in table 4.16.

Table 4. 16 The gamma passing rates of 3%, 2mm criteria of VMAT-SBRT plans irradiation with different tumor sizes.

Tumor size (cm)	Gamma passing rate of 3%, 2mm (%)
	(Static vs Dynamic mode)
1	43.80
2	43.20
3	44.30
Average	43.77
Standard deviation	0.55

#### 4.3.7 Dose test

The gamma passing rates of 3%, 2mm and criteria of VMAT-SBRT plans irradiation with different doses as shown in table 4.17. Figure 4.13 exhibits an increasing of gamma passing rates with lower doses especially in small doses of 3, 6, and 12 Gy. However, the dose differences were quite constant at high dose region. The correlation curve illustrates the positive direct variation of the mathematical linear equation together with  $R^2$  closely to 1.

Table 4. 17 The gamma passing rates of 3%, 2mm criteria of VMAT-SBRT plans irradiation with different doses.

Calculated dose (Gy)	Static measured dose (Gy)	Dose difference (%) (Plan vs Static)	Dynamic measured dose (Gy)	Dose difference (%) (Static vs Dynamic)	Total treatment time (min)
3.13	3.01	3.55	2.81	6.84	1.00
6.25	6.01	3.83	5.67	5.70	1.00
12.50	11.93	4.60	11.45	3.97	1.22
18.75	17.91	4.51	17.21	3.89	1.82
25.00	23.94	4.24	23.14	3.35	2.42
50.00	48.16	3.68	46.26	3.96	4.48
75.00	72.00	4.00	69.32	3.72	7.26
Average				4.49	2.74
Standard deviation				1.28	2.34

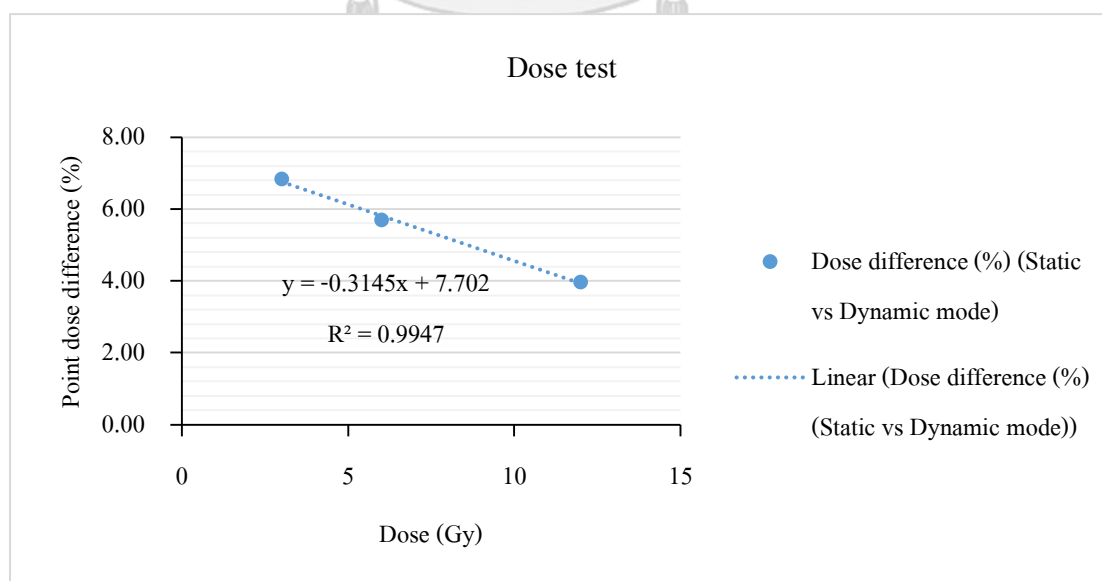


Figure 4. 13 The correlation curves of 3D moving patterns between the gamma passing rates and the different dose.

#### 4.3.8 Dose rate test

The gamma passing rates of 3%, 2mm criteria of VMAT-SBRT plan irradiation with different dose rates revealed a constant trend of the results as shown in table 4.18.

Table 4. 18 The gamma passing rates of VMAT-SBRT planned irradiation with different dose rates of 3%, 2mm.

Dose rate (MU/min)	Gamma passing rate of 3%, 2mm (%)
	(Static vs Dynamic mode)
4	40.60
8	40.60
12	38.70
14	40.50
Average	40.10
Standard deviation	0.93

#### 4.3.9 No. of fraction test

The gamma passing rates of 3%, 2mm criteria of VMAT-SBRT plans irradiation with different of no. of fractions revealed a constant trend of the results as shown in table 4.19.

Table 4. 19 The gamma passing rates of VMAT-SBRT planned irradiation with different fractions at 3%, 2mm.

No. of fraction	Calculated dose (Gy)	Static measured dose (Gy)	Dose difference (%) (Plan vs Static)	Cumulative dynamic measured dose (Gy)	Dose difference between fraction (Gy)	Dose difference (%) (Static vs Dynamic)
1				5.76	-	4.51
2				11.51	5.76	4.51
3	6.25	6.03	3.55	17.28	5.76	4.40
4				23.05	5.77	4.25
5				28.81	5.76	4.51
Average						4.43
Standard deviation						0.11

#### 4.3.10 No. of arc test

The gamma passing rates of 3%, 2mm criteria of VMAT-SBRT plans irradiation with different number of arc revealed a constant trend of the results as shown in table 4.20.

Table 4. 20 The gamma passing rates of 3%, 2mm criteria of VMAT-SBRT plans irradiation with different numbers of arcs.

No. of arc	Gamma passing rate of 3%, 2mm (%)	MU of acr1	MU of acr2	MU of acr3	Total MU
1	48.30	865	-	-	865
2	49.70	434	436	-	870
3	49.70	298	293	297	888
Average	49.23		-		
Standard deviation	0.81		-		



#### 4.3.11 Plan complexity (MU/Gy)

The gamma passing rates of 3%, 2mm criteria of VMAT-SBRT plans irradiation with different MU/Gy revealed a constant trend of the results as shown in table 4.21.

Table 4. 21 The gamma passing rates of 3%, 2mm criteria of VMAT-SBRT plans irradiation with different plan complexity.

MU/Gy	Calculated dose (Gy)	Dose difference		Dynamic measured dose (Gy)	Dose difference (%) (Static vs Dynamic)
		Static measured dose (Gy)	(%) (Plan vs Static)		
41.50	13.59	13.20	2.92	12.85	2.63
60.72	16.04	15.58	2.91	14.99	3.77
74.47	20.67	19.76	4.40	19.18	2.93
92.67	7.62	7.89	3.61	7.61	3.61
97.70	10.62	10.31	2.97	10.00	2.97
130.13	20.23	19.69	2.64	19.20	2.49
Average					3.07
Standard deviation					0.52

#### 4.4 Novel interplay effects factor (IEF) calculation

According to the results of the second experiment, it seems clear that there were three parameters of dimension, amplitude, and dose level, which significantly affect the interplay effects of VMAT-SBRT lung cancer. Therefore, in this study, we have the correlation between these parameters and IEF as shown in equation 4.1.

$$\text{IEF} = \text{Dimension} \times \text{Amp}_x \times \text{Amp}_y \times \text{Amp}_z \times \text{Dose} \quad (4.1)$$

Where Dimension defined as the dimension of tumor motion such as 1D, 2D, or 3D

Amp is the amplitude of tumor motion in X, Y, and Z directions (cm)

Dose is the prescribed dose that patient received in Gy unit

Then, the scale of scores for each dimension, amplitudes, and dose parameters were defined according to the results as presented in table 4.22, 4.23, and 4.24, respectively. To test the IEF

equation and to find out an ideal and the best cut point of IEF, the 29 clinical retrospective cases who underwent lung SBRT treatment were applied as illustrated in table 4.25.

The IEF parameter consists of the three above mentioned factors. However, the main factor influencing the interplay effects of lung VMAT-SBRT is the breathing amplitude. Refer to the results of this study, the breathing amplitudes above 5 mm lead to significant changes in gamma passing rate below 50% as displayed in table 4.23, while changing the percent point dose difference in doses as displayed in table 4.24. were within around 5%, which can be accepted. Thus, the amplitudes were used as the key factor to evaluate the cut point of IEF. Table 4.25 shows the patient no. 1 to 13, no one has amplitude of tumor travel exceeds 5 mm, the maximum IEF score of the first 13 patients was 10.13. whereas the patients ranged in age from 14 to 29, had one side of the tumor move more than 5 mm, and had a variable IEF score ranging from 2.50 to 30.00. Consequently, 10.13 was the suitable number to be used as the cut point of lung VMAT-SBRT. However, if some cases provide the IEF score of less than 10.13 but have one side of tumor motion exceeding 5 mm the applying of respiratory motion management must be considered. In addition, 1 was a perfect score of IEF, since breathing amplitude was equal or lower than 1 mm, tumor motion in only one direction, and the higher dose level was more than 12 Gy.

Table 4. 22 The scaling of score for tumor motion dimension parameter.

Dimension	Slop of linear equation	Score
1D	3.10	1.00
2D	3.44	1.00
3D	4.64	2.00

Table 4. 23 The scaling of score for breathing amplitude parameters.

Amplitude (mm)	Gamma passing rate (%)	Score
$\leq 1$	>90	1.00
2 to 5	>80	1.50
6 to 10	>50	2.00
>10	<50	2.50

Table 4.24 The scaling of score for dose level parameters.

Dose (Gy)	Dose difference (%)	Score
$\leq 3.0$	6.84	2.00
3.1 to 11.9	5.70	1.50
$\geq 12.0$	3.68	1.00

Table 4. 24 The clinical information and the IEF score of 29 lung SBRT patients were applied.

Pt. No.	Longest tumor motion distance (cm)			Dimension	Dose (Gy)	Score					
	X	Y	Z			X	Y	Z	Dimension	Dose	IEF
1	0.27	0.19	0.48	3	11.50	1.50	1.50	1.50	2.00	1.50	10.13
2	0.16	1.35	$\leq 0.10$	2	12.50	1.50	2.50	1.00	1.00	1.00	3.75
3	0.14	0.16	0.14	3	12.50	1.50	1.50	1.50	2.00	1.00	6.75
4	$\leq 0.10$	1.65	$\leq 0.10$	1	7.00	1.00	2.50	1.00	1.00	1.50	3.75
5	0.26	1.49	$\leq 0.10$	2	12.00	1.50	2.50	1.00	1.00	1.00	3.75
6	0.42	1.23	$\leq 0.10$	2	12.00	1.50	2.50	1.00	1.00	1.00	3.75
7	0.34	0.38	0.23	3	12.00	1.50	1.50	1.50	2.00	1.00	6.75
8	0.22	0.30	0.36	3	12.50	1.50	1.50	1.50	2.00	1.00	6.75
9	0.54	1.10	0.76	3	7.00	2.00	2.50	2.00	2.00	1.50	30.00
10	0.13	0.25	0.24	3	15.00	1.50	1.50	1.50	2.00	1.00	6.75
11	0.25	0.40	0.16	3	12.50	1.50	1.50	1.50	2.00	1.00	6.75
12	$\leq 0.10$	0.87	0.30	2	12.50	1.00	2.00	1.50	1.00	1.00	3.00
13	0.29	0.33	0.37	3	10.00	1.50	1.50	1.50	2.00	1.50	10.13
14	0.19	0.56	0.61	3	10.00	1.50	2.00	2.00	2.00	1.50	18.00
15	$\leq 0.10$	0.15	0.13	2	10.00	1.00	1.50	1.50	1.00	1.50	3.38
16	0.39	1.48	0.49	3	12.00	1.50	2.50	1.50	2.00	1.00	11.25
17	0.35	1.74	0.39	3	10.00	1.50	2.50	1.50	2.00	1.50	16.88
18	0.50	$\leq 0.10$	0.47	2	11.00	1.50	1.00	1.50	1.00	1.50	3.38
19	$\leq 0.10$	0.68	$\leq 0.10$	1	10.00	1.00	2.00	1.00	1.00	1.50	3.00
20	0.44	1.54	0.79	3	12.50	1.50	2.50	2.00	2.00	1.00	15.00
21	0.25	1.10	0.38	3	12.50	1.50	2.50	1.50	2.00	1.00	11.25
22	0.14	0.24	0.18	3	18.00	1.50	1.50	1.50	2.00	1.00	6.75
23	0.26	0.21	0.15	3	15.00	1.50	1.50	1.50	2.00	1.50	10.13
24	$\leq 0.10$	0.25	$\leq 0.10$	1	10.00	1.00	1.50	1.00	1.00	1.50	2.25
25	0.34	1.20	0.37	3	10.00	1.50	2.50	1.50	2.00	1.50	16.88
26	0.29	0.45	0.31	3	7.00	1.50	1.50	1.50	2.00	1.50	10.13
27	0.12	0.22	0.13	3	9.00	1.50	1.50	1.50	2.00	1.50	10.13
28	0.30	0.67	0.30	3	10.00	1.50	2.00	1.50	2.00	1.50	13.50
29	$\leq 0.10$	0.71	0.24	2	10.00	1.00	2.00	1.50	1.00	1.50	4.50

## CHAPTER 5

### DISCUSSION AND CONCLUSIONS

#### 5.1 Discussion of experiment part1

In this study, the percent of dose variation caused by the interplay effects was defined as the percent of the gamma passing rates of 1%, 1 mm with 10% threshold. Thus, increasing the percent of gamma passing rates can be interpreted as a reduction of the impact of dosimetric parameters, which leads to an interplay effect. The results showed three tendencies of the standard plan for dose measurement.

First, the decrement trend was shown in amplitude outcomes. Because the increasing of tumor amplitude can easily provide the tumor to escape from the beam trajectory. The results are in accordance with previous experimental research by Pawiro SA et al. (4), Adamczyk M et al. (5), Kakakhel MB et al. (6), and Everson A et al. (7), which stated that the interplay effects were larger for higher breathing amplitudes of SI direction.

Second, the interplay effects were reduced by the larger field size. By cause of the larger expanding area allows more doses matching accuracy between calculated and measured doses. Kakakhel MB et al. (6) also observed the increased gamma passing rates depended on the larger width of the field size. Therefore, all findings mentioned above revealed that the longer distance and the larger number of directions of the tumor motion together with smaller treatment field size increased the interplay effects. Because the larger displacement leads to the larger area where the radiation doses do not overlap. Thereby, precise patient breathing, and treatment field verification are the most important factor to ensure correct planning and delivery for lung cancer treatment.

Third, the parameters of phases, doses, dose rates, and number of fractions were not affected by the interplay effects because a simple 3D-CRT planning technique was performed in this research. This technique provides a homogeneous field without any unchanging beam intensity. Another perspective from Court LE et al. (32) is that the decrease in dose variation was associated with the decrease in dose rate. The 3D-CRT plans were generated with a dose rate of 300 MU/min, which was less than twice the dose rate used in IMRT and VMAT. However, lowering the dose rate

leads to prolonged treatment times, increasing the likelihood of patient motion during the treatment delivery (33).

## 5.2 Discussion of experiment part2

In this part, the percent of dose variation caused by the interplay effects was defined as the percent of the gamma passing rate of 3%, 2 mm, following the criteria of AAPM task group number 218 (31) recommendation for SBRT planning technique, and the percent of the point dose difference. Thus, increasing the percent of both indexes can be interpreted as a reduction of the impact of dosimetric parameters to an interplay effect. The results also presented show the variety of outcomes for each parameter, which affected the VMAT-SBRT plans dose measurement.

First, breathing pattern and tumor dimension, the decrement trend of both breathing amplitude and dimension. Because the increasing of tumor amplitude can provide field dose blurring as well as field dose error between calculated and measured doses. This reason lead to the reduction of percent of gamma passing rate of higher motion. The results agreed with our results in the first part of the experiment, in which, the higher breathing amplitudes and tumor motion dimension brought out the appearance of larger interplay effects. Obviously, when comparing the results among three dimensions of tumor moving as displayed in the figure 4.12. The slope value of the XYZ-amplitude correlation curve of this study shows the  $R^2$  value more than the  $R^2$  value of both X-amplitude, Y-amplitude, Z-amplitude, XY-amplitude, and XZ-amplitude, whereas these six curves still receive the resemble outcomes. This point indicated that the 3D amplitude motion has more impact on the interplay effects than the 1D and 2D amplitude motions. By the reason of more tumor motion direction will cause more chance of radiation dose distortion within the radiation field. Furthermore, SBRT cases provide the dose rapid fall-off within the treatment field. Hence, a few mismatches between calculated and measured doses can lead to interplay effects. Therefore, 3D is the most impact for VMAT-SBRT cases. Nevertheless, this research found no correlation between the increase in breathing phase and dose validation due to the interplay effect.

Second, tumor size and the increase in tumor size did not affected the interplay effects. Edvardsson A et al. (7) also revealed the magnitude of the dosimetric effect of interplay did not vary much between different CTV sizes. The size of the hot- and cold spots in their simulated dose

distributions is approximately the same irrespective of the CTV size, as the width of the MLC is the same.

Third, dose level and dose rate, the reduction of interplay effects by the smaller doses. Because shorter treatment time provides lesser of dose smearing between calculated and measured doses distribution as shown in table 4.17. The lower doses of 3, 6, and 12 Gy provide average treatment time in 1 min, while higher doses allowed longer than 1 min of time treatment. These outcomes agreed with Edvardsson A et al. (7), which they explained that the longer delivery times imply that more respiratory cycles will pass during the treatment delivery. Furthermore, the dose rate study can be explained by the reason of treatment time as well, since the higher dose rate can provide a shorter time treatment. Likewise, Edvardsson A et al. study (7) showed the delivery time of 2 Gy FFF, 2 Gy FF, 10 Gy FFF, and 10 Gy FF the treatment times were 1.00, 1.06, 2.50, and 5.16 min, respectively. Ong CL et al. (33) illustrated the increasing of interplay effects for FFF compared to FF VMAT-SBRT treatment technique. Court LE et al (32) presented the increasing trend of interplay effects for higher dose rates for IMRT treatment technique. However, in this study cannot fix the dose rates due to the VMAT planning property. Therefore, our results of different dose rates did not impact the interplay effects.

Forth, various no. of arc and fractionation were not affected by the interplay effects. Because the increase of the number of arcs was compensated for the lower MU, as shown in table 4.20. As a result, all half arcs received close to the total monitor unit value. Because the similarity of VMAT-SBRT treatment planning and phantom moving pattern were used in each fraction, the number of fractions studied was increased. Therefore, the dose discrepancy due to the interplay effects was not found.

Fifth, plan complexity (MU/Gy), the increment plan complexity was not observed in this study because of the dose compensation between hot and cold spots during irradiation. Besides, only middle point dose measurements were applied in this study. This result is similar to that of Gotstedt J et al (34). They also interpreted that it would be possible to increase the number of MU/Gy for a treatment plan without actually increasing the complexity, and more advanced complexity metrics could be used. In contrast with Ong CL et al (33) studies, they observed that the interplay effects increased for a higher number of MU/Gy. However, they also mentioned that the number of MU/Gy may not be a perfect measure of the plan complexity, since there is more

MLC movement and smaller field openings. Nevertheless, the interplay effect in clinical plans cannot be deliberated for some specific parameters, but all dosimetric parameters of each case should be considered. Edvardsson A et al. (7) also indicated that the large interplay effect was observed for individual fractions and the extent varied with patient and machine-specific parameters. Each patient has a unique respiratory pattern that affects the particular planning parameters. These reasons explain the different mutual movements between the target and the MLC, resulting in a different extent of the interplay effects.

### **5.3 Discussion of novel IEF calculation**

The IEF in this research was derived from the concept of Kubo et al.'s study (15), which calculated the interplay effect variable score (IVS) from the combination of the complexity of the MLC sequence (TMMCSv), the amplitude of the tumor in one direction, and the number of patients breathing. Nevertheless, our results revealed the three parameters of dimension and amplitude of tumor motion, including dose level, are the most critical concerns for lung VMAT-SBRT during irradiation, especially for amplitudes. According to the outcomes, breathing amplitudes above 5 mm lead to significant changes in gamma passing rate below 50%, as displayed in figure 4.12, which results in a change in the shape of dose distribution due to the interplay effects, especially for 3D movements.

To reduce the dose discrepancy during irradiation, respiratory motion management (RMM) must be applied, especially in advanced treatment techniques that provide high dose gradient plans such as VMAT-SBRT. Thus, the use of RMM makes it possible to reduce the irradiated area and lower the incidence of adverse effects in principle. Our results were similar to the recommendation of AAPM task group 76 (18). The suggestion is that tumor motion should be measured for each patient for whom respiratory motion is a concern. If target motion is greater than 5 mm, a method of respiratory motion management is available, and if the patient can tolerate the procedure, respiratory motion management technology is appropriate.

## Conclusions

The interplay effects for 6 MV FFF photon beams in VMAT-SBRT lung cancer are more pronounced for the higher amplitudes and the smaller doses. The breathing amplitudes above 5 mm lead to significant changes in the shape of dose distribution due to the interplay effects especially for 3D movements. The novel IEF is a parameter that can indicate the interplay effects directly for VMAT-SBRT lung cancer patients. The value of 1 is the ideal score of IEF, while the value more than 10.13 is the score that can imply the need of respiratory motion management. However, the score is lower than 10.13, but that case provides some tumor motion exceeds 5 mm in any direction, the need for respiratory motion management was also recommended.



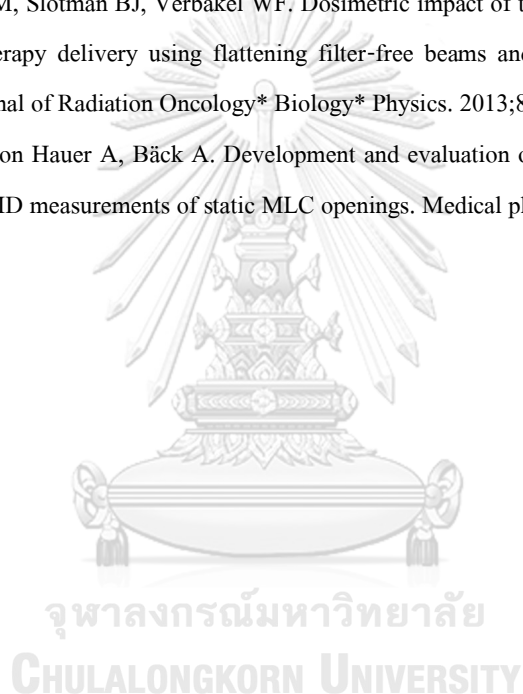


## REFERENCES

1. Sung H, Ferlay J, Siegel RL, Laversanne M, Soerjomataram I, Jemal A, et al. Global cancer statistics 2020: GLOBOCAN estimates of incidence and mortality worldwide for 36 cancers in 185 countries. *CA: a cancer journal for clinicians*. 2021;71(3):209-49.
2. Tsang MW. Stereotactic body radiotherapy: current strategies and future development. *Journal of thoracic disease*. 2016;8(Suppl 6):S517.
3. John C, Dal Bello R, Andratschke N, Guckenberger M, Boda-Heggemann J, Gkika E, et al. In-field stereotactic body radiotherapy (SBRT) reirradiation for pulmonary malignancies as a multicentre analysis of the German Society of Radiation Oncology (DEGRO). *Scientific reports*. 2021;11(1):1-11.
4. Pawiro S, editor *Dosimetric impact of interplay effect in lung IMRT and VMAT treatment using in-house dynamic thorax phantom*. *Journal of physics: Conference series*; 2016: IOP Publishing.
5. Adamczyk M, Adamczyk S, Piotrowski T. Modelling the effects of lung cancer motion due to respiration. *Nukleonika*. 2020;65.
6. Kakakhel MB, Kairn T, Kenny J, Seet K, Fielding A, Trapp J. Interplay effects during enhanced dynamic wedge deliveries. *Physica Medica*. 2013;29(4):323-32.
7. Edvardsson A, Nordström F, Ceberg C, Ceberg S. Motion induced interplay effects for VMAT radiotherapy. *Physics in Medicine & Biology*. 2018;63(8):085012.
8. Ehrbar S, Perrin R, Peroni M, Bernatowicz K, Parkel T, Pytko I, et al. Respiratory motion-management in stereotactic body radiation therapy for lung cancer—A dosimetric comparison in an anthropomorphic lung phantom (LuCa). *Radiotherapy and oncology*. 2016;121(2):328-34.
9. Riley C, Yang Y, Li T, Zhang Y, Heron DE, Huq MS. Dosimetric evaluation of the interplay effect in respiratory-gated RapidArc radiation therapy. *Medical physics*. 2014;41(1):011715.
10. Vassiliev ON, Kry SF, Chang JY, Balter PA, Titt U, Mohan R. Stereotactic radiotherapy for lung cancer using a flattening filter free Clinac. *Journal of applied clinical medical physics*. 2009;10(1):14-21.
11. Aoki S, Yamashita H, Haga A, Nawa K, Imae T, Takahashi W, et al. Flattening filter-free technique in volumetric modulated arc therapy for lung stereotactic body radiotherapy: A clinical comparison with the flattening filter technique. *Oncology letters*. 2018;15(3):3928-36.
12. Georg D, Knöös T, McClean B. Current status and future perspective of flattening filter free photon beams. *Medical physics*. 2011;38(3):1280-93.
13. Sharma SD. Unflattened photon beams from the standard flattening filter free accelerators for radiotherapy: advantages, limitations and challenges. *Journal of Medical Physics/Association of Medical Physicists of India*. 2011;36(3):123.

14. Dang TM, Peters MJ, Hickey B, Semciw A. Efficacy of flattening-filter-free beam in stereotactic body radiation therapy planning and treatment: A systematic review with meta-analysis. *Journal of medical imaging and radiation oncology*. 2017;61(3):379-87.
15. Kubo K, Monzen H, Tamura M, Hirata M, Ishii K, Okada W, et al. Minimizing dose variation from the interplay effect in stereotactic radiation therapy using volumetric modulated arc therapy for lung cancer. *Journal of applied clinical medical physics*. 2018;19(2):121-7.
16. McNiven AL, Sharpe MB, Purdie TG. A new metric for assessing IMRT modulation complexity and plan deliverability. *Medical physics*. 2010;37(2):505-15.
17. Masi L, Doro R, Favuzza V, Cipressi S, Livi L. Impact of plan parameters on the dosimetric accuracy of volumetric modulated arc therapy. *Medical physics*. 2013;40(7):071718.
18. Keall PJ, Mageras GS, Balter JM, Emery RS, Forster KM, Jiang SB, et al. The management of respiratory motion in radiation oncology report of AAPM Task Group 76 a. *Medical physics*. 2006;33(10):3874-900.
19. society Ac. About lung cancer 2019, October 1 [Available from: <https://www.cancer.org/cancer/lung-cancer/about/what-is.html>. .
20. Khan FM, Gibbons JP. *Khan's the physics of radiation therapy*: Lippincott Williams & Wilkins; 2014.
21. Prescribing I. Recording and reporting photon beam therapy. ICRU Report 50. Bethesda, MD: International Commission on Radiation Units and Measurements. 1993.
22. Morgan-Fletcher S. Prescribing, recording and reporting photon beam therapy (Supplement to ICRU Report 50), ICRU Report 62. ICRU, pp. ix+ 52, 1999 (ICRU Bethesda, MD) \$65.00 ISBN 0-913394-61-0. British Institute of Radiology; 2001.
23. Benedict SH, Yenice KM, Followill D, Galvin JM, Hinson W, Kavanagh B, et al. Stereotactic body radiation therapy: the report of AAPM Task Group 101. *Medical physics*. 2010;37(8):4078-101.
24. Klein EE, Hanley J, Bayouth J, Yin FF, Simon W, Dresser S, et al. Task Group 142 report: Quality assurance of medical accelerators a. *Medical physics*. 2009;36(9Part1):4197-212.
25. Medicine P. Breathing cycle 2017 [Available from: <http://www.pathwaymedicine.org/breathing-cycle>. .
26. detector R. Solid-state detector. 2021 [Available from: <https://www.britannica.com/science/solid-state-detector>. .
27. Niroomand-Rad A, Blackwell CR, Coursey BM, Gall KP, Galvin JM, McLaughlin WL, et al. Radiochromic film dosimetry: recommendations of AAPM radiation therapy committee task group 55. *Medical physics*. 1998;25(11):2093-115.
28. Ezzell GA, Burmeister JW, Dogan N, LoSasso TJ, Mechalakos JG, Mihailidis D, et al. IMRT commissioning: multiple institution planning and dosimetry comparisons, a report from AAPM Task Group 119. *Medical physics*. 2009;36(11):5359-73.

29. Low DA, Harms WB, Mutic S, Purdy JA. A technique for the quantitative evaluation of dose distributions. *Medical physics*. 1998;25(5):656-61.
30. PHILIPS. Big Bore RT 2021 [Available from: <https://www.philips.co.th/healthcare/product/HC728242/big-bore-rt>].
31. Miften M, Olch A, Mihailidis D, Moran J, Pawlicki T, Molineu A, et al. Tolerance limits and methodologies for IMRT measurement-based verification QA: recommendations of AAPM Task Group No. 218. *Medical physics*. 2018;45(4):e53-e83.
32. Court LE, Wagar M, Ionascu D, Berbeco R, Chin L. Management of the interplay effect when using dynamic MLC sequences to treat moving targets. *Medical physics*. 2008;35(5):1926-31.
33. Ong CL, Dahele M, Slotman BJ, Verbakel WF. Dosimetric impact of the interplay effect during stereotactic lung radiation therapy delivery using flattening filter-free beams and volumetric modulated arc therapy. *International Journal of Radiation Oncology\* Biology\* Physics*. 2013;86(4):743-8.
34. Götstedt J, Karlsson Hauer A, Bäck A. Development and evaluation of aperture-based complexity metrics using film and EPID measurements of static MLC openings. *Medical physics*. 2015;42(7):3911-21.



## APPENDIX

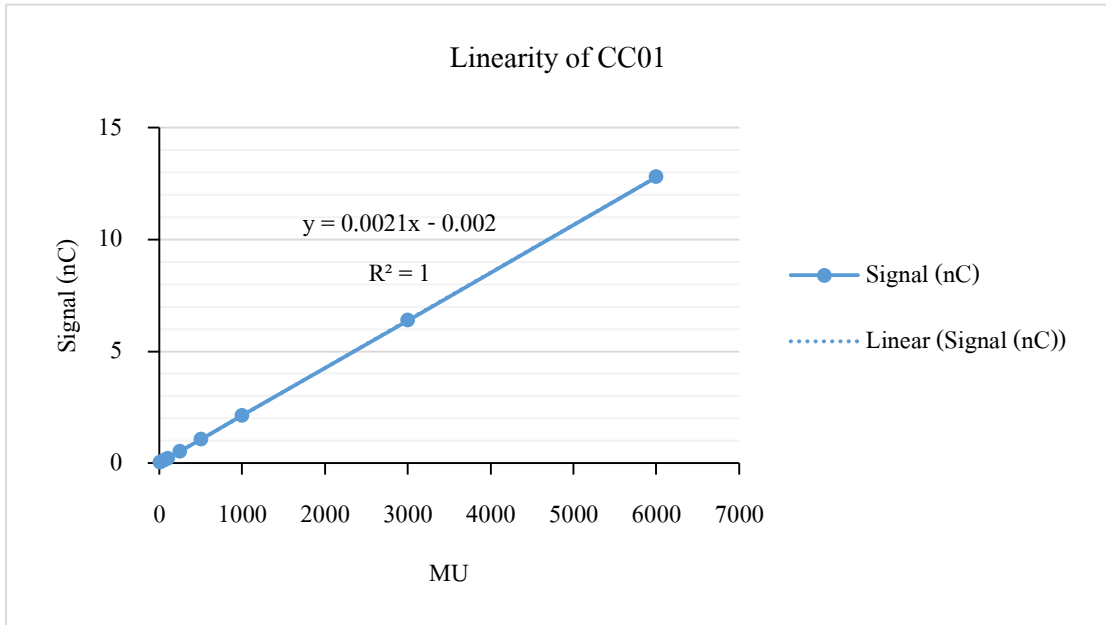
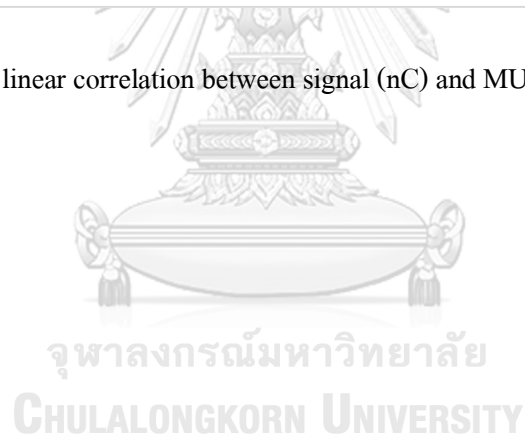


Figure A. 1 The linear correlation between signal (nC) and MU of linearity test of CC01.



## VITA

**NAME** Vanida Poolnapol  
**DATE OF BIRTH** 2 June 1993  
**PLACE OF BIRTH** Chonburi  
**INSTITUTIONS ATTENDED** Master of Science  
**HOME ADDRESS** 49/69 Moo 9 Bangpha Siracha Chonburi 20110



จุฬาลงกรณ์มหาวิทยาลัย  
CHULALONGKORN UNIVERSITY